NAVAL POSTGRADUATE SCHOOL

MONTEREY, CALIFORNIA

THESIS

RADAR POLARIMETRY

by

Yong, Siow Yin

December 2004

Thesis Advisor:	Brett Borden
Second Reader:	Donald Walters

Approved for public release; distribution is unlimited

THIS PAGE INTENTIONALLY LEFT BLANK

REPORT DOCUMENTATION PAGE			*Form Approved OMB No. 0704-0188*
Public reporting burden for this collection of information is estimated to average 1 hour per response, including the time for reviewing instruction, searching existing data sources, gathering and maintaining the data needed, and completing and reviewing the collection of information. Send comments regarding this burden estimate or any other aspect of this collection of information, including suggestions for reducing this burden, to Washington headquarters Services, Directorate for Information Operations and Reports, 1215 Jefferson Davis Highway, Suite 1204, Arlington, VA 22202-4302, and to the Office of Management and Budget, Paperwork Reduction Project (0704-0188) Washington DC 20503.			
1. AGENCY USE ONLY *(Leave blank)*	**2. REPORT DATE** December 2004	**3. REPORT TYPE AND DATES COVERED** Master's Thesis	
4. TITLE AND SUBTITLE: Radar Polarimetry		**5. FUNDING NUMBERS**	
6. AUTHOR(S) Yong Siow Yin			
7. PERFORMING ORGANIZATION NAME(S) AND ADDRESS(ES) Naval Postgraduate School Monterey, CA 93943-5000		**8. PERFORMING ORGANIZATION REPORT NUMBER**	
9. SPONSORING /MONITORING AGENCY NAME(S) AND ADDRESS(ES) N/A		**10. SPONSORING/MONITORING AGENCY REPORT NUMBER**	
11. SUPPLEMENTARY NOTES The views expressed in this thesis are those of the author and do not reflect the official policy or position of the Department of Defense or the U.S. Government.			
12a. DISTRIBUTION / AVAILABILITY STATEMENT Approved for public release; distribution is unlimited		**12b. DISTRIBUTION CODE**	

13. ABSTRACT (maximum 200 words)

Radar polarimetry is a recent development seeing active research only in the last few decades. The phenomenon that optimal (maximal power) reflected fields exist in both the co-polarized and cross polarized channels of the receiving radar antenna was first introduced by Kennaugh and Huynen. Current research efforts focus on target scattering matrices and relating them to physical attributes of the target. This thesis provides a comprehensive survey of the polarimetry theories that have been put forth by various researchers to characterize, manipulate and optimize target radar returns via polarization states. One such theory is the Target Decomposition (TD) theorem that seeks to decompose the target returns into individual scattering mechanisms. The topic of optimization of polarization states of the incident field for maximizing power return is also examined. Two models are implemented in Matlab to verify and demonstrate these polarimetry theories. The first model uses TD theorems to simulate foliage clutter and study its effect on the polarization of the incident electric field. A (simulated) static dihedral target is introduced and its effect on wave polarization is also simulated. The second model studies optimization of polarization states. Both models are able to produce the expected results for known canonical targets.

14. SUBJECT TERMS Radar, Polarimetry, Polarization, Target Decomposition Theorem, Jones vector, Stokes, Mueller, Pauli Matrices, Polarization States Optimization			**15. NUMBER OF PAGES** 89
			16. PRICE CODE
17. SECURITY CLASSIFICATION OF REPORT Unclassified	**18. SECURITY CLASSIFICATION OF THIS PAGE** Unclassified	**19. SECURITY CLASSIFICATION OF ABSTRACT** Unclassified	**20. LIMITATION OF ABSTRACT** UL

THIS PAGE INTENTIONALLY LEFT BLANK

RADAR POLARIMETRY

Siow Yin Yong
Civilian, Republic of Singapore
B.Eng., National University of Singapore, 1998

Submitted in partial fulfillment of the
requirements for the degree of

MASTER OF SCIENCE IN COMBAT SYSTEMS TECHNOLOGY

from the

**NAVAL POSTGRADUATE SCHOOL
December 2004**

Author: Yong Siow Yin

Approved by: Professor Brett Borden
               Thesis Advisor

               Professor Donald Walters
               Second Reader/Co-Advisor

               Professor James Luscombe
               Chairman, Department of Physics

THIS PAGE INTENTIONALLY LEFT BLANK

ABSTRACT

Radar polarimetry is a relatively recent development seeing active research only in the last few decades. The phenomenon that optimal (maximal power) reflected fields may exist in both the co-polarized and cross polarized channels of the receiving radar antenna was first introduced by Kennaugh and Huynen. Current research efforts focus on target scattering matrices relating physical attributes of the target that bring about depolarization of the scattered field so as to identify the various scattering mechanisms and to enhance target identification and detection.

This thesis provides a comprehensive survey of the polarimetry theories that have been put forth by various researchers to characterize, manipulate and optimize target radar returns via polarization states. These polarimetry theories include matrix representations of polarization, the various vector representations (Jones, Sinclair, Stokes, Mueller etc.) and their usefulness. This thesis also examines the Target Decomposition (TD) theorem that seeks to decompose the target returns into individual scattering mechanisms so that these returns can be attributed to physical characteristics of the target. Lastly, the topic of optimization of polarization states for maximizing power return is also examined.

Two separate models are implemented in Matlab to verify and demonstrate this polarimetry theory. The first model uses TD theorems to simulate foliage clutter and study its effect on the polarization of the incident electric field. As part of this analysis, a (simulated) static dihedral target is introduced and its effect on wave polarization is also simulated. The second model was constructed to study optimization of polarization states. This model takes the target scattering matrix as an input and creates all possible polarization states of incident waves to interact with this target. It then graphs the backscattered power in the co-polarized and cross-polarized channels. Both models are able to produce the expected results for known canonical targets.

THIS PAGE INTENTIONALLY LEFT BLANK

TABLE OF CONTENTS

LIST OF FIGURES

THIS PAGE INTENTIONALLY LEFT BLANK

LIST OF TABLES

THIS PAGE INTENTIONALLY LEFT BLANK

ACKNOWLEDGMENTS

I would like to thank my thesis supervisor Prof Brett Borden for his excellent technical guidance, patience and his encouragement in my pursuance of this thesis topic. Radar polarimetry has been an interesting but especially challenging topic for me given my background in mechanical engineering, but Prof Borden has been most encouraging every step of the way.

I am also grateful to Prof Walters for patiently going over my work meticulously and giving invaluable advice.

On a personal note, I am glad for the company of my fellow Singaporean students in the Sensor group. The journey of learning in NPS has indeed been a fun-filled one due to their presence.

Lastly, I would like to thank my husband, Jeffrey.

THIS PAGE INTENTIONALLY LEFT BLANK

I. INTRODUCTION

Radar polarimetry is a promising area of research - especially when remote sensing applications in Synthetic Aperture Radar (SAR) are considered. Traditionally, radars transmit and receive waveforms in the same polarization state. The measured data include the amplitude, frequency, and the differential phase of the received wave as compared to the transmitted wave.

However, when a propagating EM wave strikes a dielectric or a conducting medium, the discontinuity of the scatterer will generally act to depolarize the EM wave, possibly resulting in a completely opposite sense of polarization state of the scattered wave to which the radar receiver may be blind. All information (amplitude, frequency and phase) in the orthogonal polarization state of the back scattered wave will then be lost. The concept of depolarization can be illustrated with the example of a wire. A polarized electric field that is incident on the wire will induce currents along the wire and these currents will in turn re-radiate energy that is polarized in the direction of the wire. As illustrated in Figure I-1, the scattered wave now has a E_x component that does not exist in the incident wave. If the incident electric field is orthogonal to the direction of the wire, one would not expect a scattered wave since no currents are induced. Hence the polarization of the scattered electric field is dependent on the geometry or orientation of the wire.
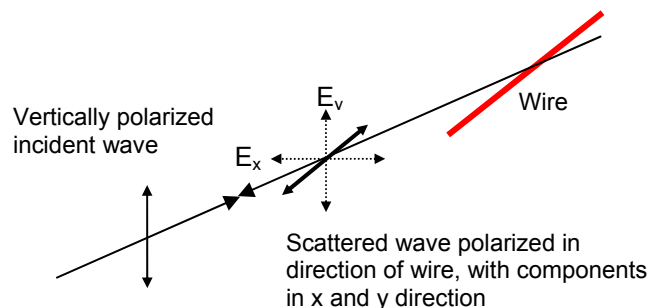
Figure I-1 Example of a wire depolarizing an incident electric field and scattered wave polarized in the direction of wire, with components in the x and y directions

A polarimetric radar has two receiving antennas with orthogonal polarization states. The emitted EM wave is scattered by the target and measured by both receivers so that both co-polarized and cross-polarized signals are determined. These measurements provide information about the physical attributes of the target. Polarization detection may also allow detection of some stealthy targets that can completely depolarize the transmitted wave, resulting in a null co-polarized power and a maximized cross-polarized power.

A.   RECENT RESEARCH AND DEVELOPMENTS

The basic principles of radar polarimetry are based on the concept of characteristic polarization states first introduced by Kennaugh [1], who demonstrated that there exist radar polarization states for which the radar receives maximum or minimum power and how these states can be optimized. Hence the backscatter power of the target depends on the polarization state of the incident electric fields. Many techniques have been developed to determine the optimal polarization state and involve manipulation of the target scattering matrices. The results are usually expressed in terms of the power received by the cross-polarized and the co-polarized channels and illustrate the importance of a full polarimetric data set for deriving target information.

Kennaugh's work was followed by Huynen's [2] study of how targets geometrical properties and physical structure can be determined by their back scattered polarization states. Current researchers, including Boerner and Cloude [1], [2], [4] & [5], have expanded on the concept of Target Decomposition theorems that serve to extract information about the target. The main idea is to express the average scattering matrix for a random medium as a sum of independent elements and to associate a physical scattering mechanism with each of these independent elements. These research efforts also aim to integrate multi-polarization data into multi-temporal, multi-frequency data of SAR interferometry (POLINSAR) so as to achieve greater target resolution, clutter suppression and increased detection probability.

2

The following C-band images of agricultural fields demonstrate the dependence of the radar's response to polarization (Figure I-2). The top two images are like-polarized (HH on left, VV on right), and the lower left image is cross-polarized (HV). The lower right image is the result of displaying these three images as a color composite (in this case, HH - red, VV - blue, and HV - green).
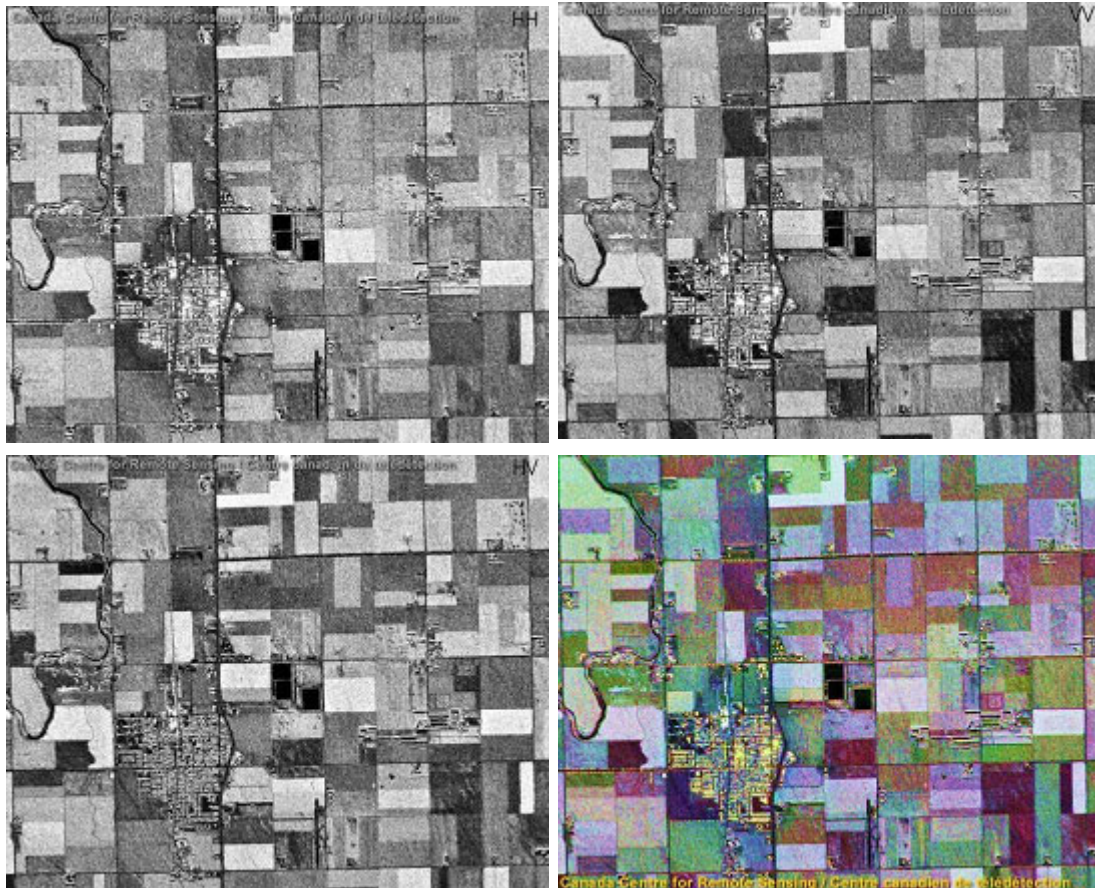
Figure I-2 Illustration of how different polarizations (HH, VV, HV & color composite) bring out different features in an agricultural scene [9]. (In the color plot, HH is red, VV is blue and HV is green)

In terms of actual applications, Table 1 gives some of the current developments or missions employing polarimetric radars in remote sensing.

Table I-1 Polarimetrc Radars

Mission	Application	Polarization
JPOLE	Weather radar by NSSL	-
SIR-C	Remote Sensing on Satellite	HH,HV,VV,VH
ALOS	Remote Sensing on Satellite	HH,HV,VV,VH

B.   THESIS OUTLINE

This thesis seeks to examine and verify the polarization concepts and models put forth by the current researchers. The author will make use of the following polarimetry theories:

1. Electromagnetic wave propagation and polarization;

2. Various scattering matrices of man-made or natural objects and their relationship to the physical geometries of these objects;

3. Target decomposition (TD) theorems and their basis in scattering physics. TD theorems will be used to introduced physical variations into scattering matrices;

4. Optimization of polarization states for various target scattering matrices in response to various incident electric fields. Polarization optimization results in maximal/minimal power received by the receiving antenna, in both the co- and cross- polarized channels and this is unique for each target.

Theoretical analyses of the above research subjects will be conducted using Matlab codes to investigate the behavior of various targets. The analysis will be conducted primarily based on TD theorems and polarization optimization, respectively. To demonstrate the TD theorems, the scenario of a stationary

dihedral scatterer and other canonical targets hidden in foliage clutter will be examined and polarimetry will be employed as the primary tool for target detection. To examine polarization optimization, an analytical technique used currently to determine optimal polarization states will be implemented in Matlab. The resulting model will be able to generate the optimal polarization states for the incident electric field for a given input target resulting in maximized/minimized power in the co-polarized and cross-polarized channels.

Chapter II will address the behavior of EM wave propagation and interaction with surfaces. Here we will illustrate the idea of depolarization from interaction between the EM wave and the scatterer due to the physical attributes of the scatterer.

Chapter III illustrates the various concepts used in Polarimetry Theory. These include tools used to determine the polarization states of scattered EM waves due to interaction with natural or man-made scatterers and their theoretical basis.

Chapter IV describes the details of the theoretical analyses conducted and implemented in Matlab. This chapter concludes with the modeling results and their analyses.

THIS PAGE INTENTIONALLY LEFT BLANK

II. ELECTRMAGNETISM & POLARIZATION

A. MAXWELL'S EQUATIONS

James Clerk Maxwell (1831-1879) put together the laws of electromagnetism in the form of four equations based on theories comprising previously known experimental and theoretical results. These are given in Table II-1. Most importantly, he introduced the concept of electromagnetic *waves* and the physics that govern their propagation.

Table II-1 Maxwell's Equations [16]

Differential Form	Integral Form	
$\nabla . D = \rho_v$	$\oint_S D \cdot dS = \int_\upsilon \rho_\upsilon d\upsilon$	(2.1)
$\nabla \cdot B = 0$	$\oint_S B \cdot dS = 0$	(2.2)
$\nabla \times E = -\dfrac{\partial B}{\partial t}$	$\oint_L E \cdot dl = -\dfrac{\partial}{\partial t} \int_S B \cdot dS$	(2.3)
$\nabla \times H = J + \dfrac{\partial D}{\partial t}$	$\oint_L H \cdot dl = \int_S (J + \dfrac{\partial D}{\partial t}) \cdot dS$	(2.4)

Assuming a time factor of $e^{-j\omega t}$ and noting that $B = \mu H$, $J = \sigma E$; and taking the curl of both sides of the differential form of (2.3) gives

$$\nabla \times \nabla \times E = -j\omega\mu\nabla \times H \qquad (2.5)$$

$$\nabla(\nabla \cdot E) - \nabla^2 E = -j\omega\mu(\sigma + j\omega\varepsilon)E \qquad (2.6)$$

$$\nabla^2 E - \gamma^2 E = 0 \qquad (2.7)$$

where

$$\gamma^2 = j\omega\mu(\sigma + j\omega\varepsilon) \qquad (2.8)$$

and γ is called the propagation constant. Note that the $e^{-j\omega t}$ disappears because it is associated with every term and therefore factors out, resulting in time independent equations. By a similar process, it can be shown for the magnetic field, H, that

$$\nabla^2 H - \gamma^2 H = 0 \tag{2.9}$$

Equations (2.7) and (2.9) are known as the Helmholtz equations. The solution to the first equation gives the electric field propagation equation. We can assume that the wave propagates along the +z direction and that E has only an x-component, then

$$E = E_x(z) \tag{2.10}$$

Substituting into equation (2.7) gives

$$(\nabla^2 - \gamma^2)E_x(z) = 0$$

$$\tag{2.11}$$

$$\left[\frac{d^2}{dz^2} - \gamma^2\right]E_x(z) = 0$$

Finally, realizing that this is a linear homogeneous differential equation, we can insert the time factor and obtain the final solution as follows:

$$E(z,t) = E_0 e^{-\alpha z}\cos(\omega t - kz) \tag{2.12}$$

where E_0 is a scalar constant, α is the attenuation constant, ω is the angular frequency and k is the phase constant or the wave constant. Equation (2.12) is the electric field vector that defines the propagation of the electric field.

The magnetic field H is related to the E-field and follows by a similar argument. In a different (but equivalent form), we write

$$H(z,t) = \mathrm{Re}(H_0 e^{-\alpha z}e^{j(\omega t - kz)}) \tag{2.13}$$

$$H = \frac{E_0}{|\eta|}e^{-\alpha z}\cos(\omega t - kz + \delta) \tag{2.14}$$

where η is the intrinsic impedance and may be complex. This complex nature of η introduces a phase difference δ between E and H fields (note that this is a phase difference, assuming E-field has zero absolute phase). In free space, the E-field, H field and the direction of wave propagation are all orthogonal to each other and can be represented as in Figure II-1.
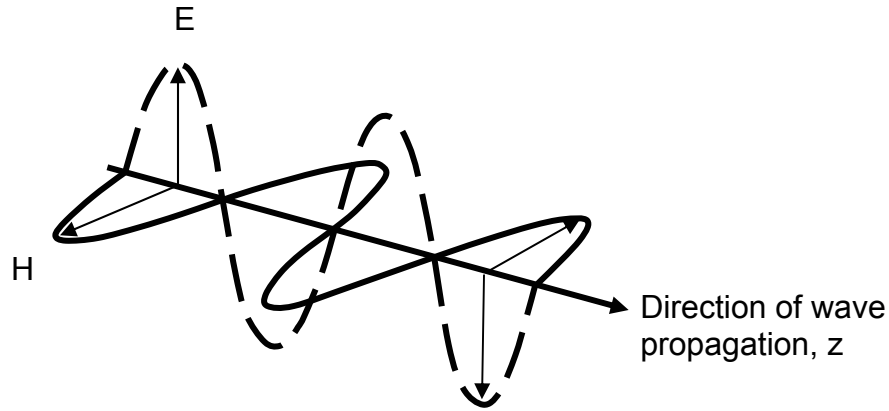
Figure II-1 Electromagnetic Wave Propagation in Free Space

B. WAVE PROPAGATION AND POLARIZATION

Having defined the electric and magnetic field vector, we now turn our attention to the interaction of EM-waves with various media. The relative amplitude of the incident, reflected and transmitted waves depends on the constitutive parameters of the two media involved, i.e. the permeability ε, permittivity, μ and the conductivity, σ. Objects that tend towards conductors reflect most of the incident wave energy, while objects that tend towards lossy dielectrics absorb larger portions of the incident energy.

In addition to energy reflection and transmission, the waves can become depolarized so that the polarization state of the incident wave differs from that of the scattered wave. Hence the resultant state of the scattered wave depends on the polarization of the incident wave as well as the parameters of the reflecting medium. We discuss the elements of wave propagation in the following sections.

9

1. Polarization

Consider an EM wave propagating out of the page and situated at the origin of an x-y axis system, as shown in Figure II-2. The E-field is represented by the vector shown and varies continuously in magnitude and changes direction every half-period according to the sinusoidal behavior described in Section II.A. The components of the E-field in the x-y directions are:

$$E(z,t) = E_x(z,t) + E_y(z,t) \tag{2.15}$$

$$E_x(z,t) = E_{0x} \cos(\omega t - kz + \delta_x) \tag{2.16}$$

$$E_y(z,t) = E_{0y} \cos(\omega t - kz + \delta_y) \tag{2.17}$$
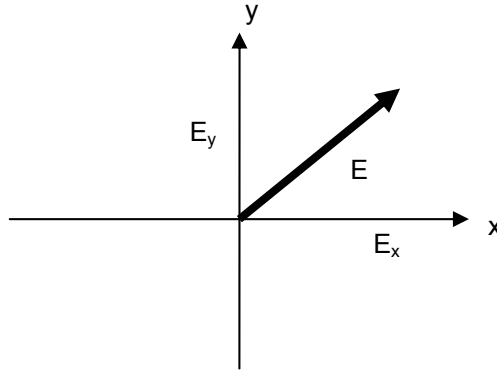
Figure II-2 Representation of instantaneous E-vector

Examining the two components E_x and E_y, shows that the sum of two sinusoidal waves traces an ellipse. Their mathematical relationship is described in the following equation of an ellipse:

$$\left(\frac{E_x}{E_{0x}}\right)^2 - 2\frac{E_x E_y}{E_{0x} E_{0y}} \cos\delta + \left(\frac{E_y}{E_{oy}}\right)^2 = \sin^2\delta \tag{2.18}$$

where $\delta = \delta_y - \delta_x$, is the phase difference between E_x and E_y.

Depending on the parameters of the ellipse equation, the E-vector may be reduced to the special cases of linearly polarized (as in Fig II-2), circularly polarized and the most general case being elliptically polarized. Linear polarization occurs when the two orthogonal components E_x and E_y are in phase and so the direction of the linear polarization depends on the relative amplitude

of the two components. Circular polarization occurs when the two orthogonal components have the same amplitude but are exactly ninety degrees out of phase. All other cases (with the two components not in phase and not having the same amplitude) are elliptical polarizations.
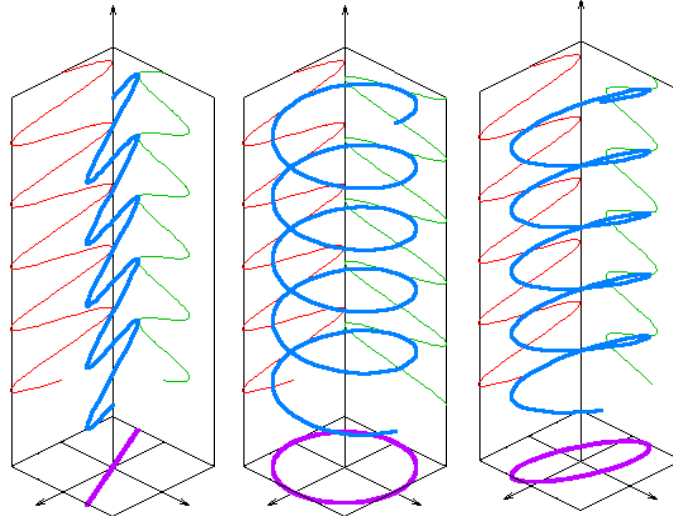
Figure II-3 Illustration of (i) Linear, (ii) Circular and (iii) Elliptical Polarization[19]

The polarization ellipse is a common representation of the state of polarization. The tilt angle, φ of the ellipse is obtained from

$$\tan 2\varphi = \frac{2E_{0x}E_{oy}\cos\delta}{E_{ox}^2 - E_{oy}^2}$$ (2.19)

The ellipticity angle, τ is simply derived from the major and minor axes of the ellipse as follows,

$$\tan\tau = \frac{Minor\ axis}{Major\ axis}$$ (2.20)
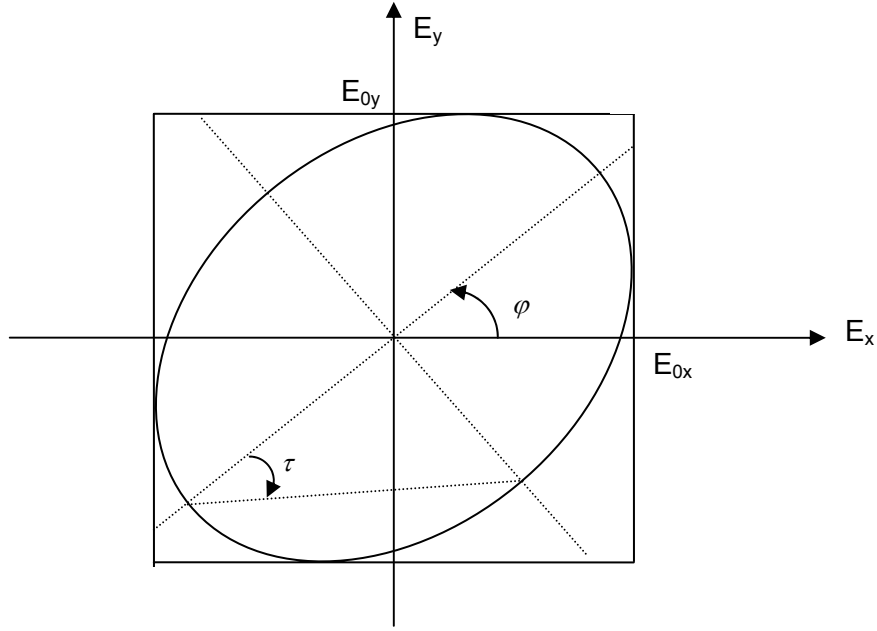
Figure II-4 The Polarization Ellipse

From Mott [11], the wave can also be characterized by more tractable mathematical terms using the polarization ratio, which is a complex number, shown here with its relation to the polarization ellipse parameters [1]

$$P = \frac{E_y}{E_x} = \frac{E_{0y}}{E_{0x}} \cdot e^{i\delta} = \tan \varphi \, e^{j\delta} = \frac{\tan \varphi + \tan \tau}{1 - j \tan \varphi \tan \tau} \qquad (2.21)$$

For a circularly polarized wave, the EM wave is a sum of equal amplitude left-hand polarized and right-hand polarized components, E_L and E_R. The polarization, after some manipulation, is then [11]

$$q = \frac{E_L}{E_R} = \frac{1 - jP}{1 + jP} \qquad (2.22)$$

Using a modified polarization ratio, $p = jP$, we then obtain,

$$q = \frac{1 - p}{1 + p}$$

$$\qquad (2.23)$$

$$p = \frac{1 - q}{1 + q}$$

The various representations provide varying degrees of ease in representing the polarization of a propagating wave and are also utilized for more

12

complex types of representations, e.g. the Poincarē sphere. A more in-depth treatment of polarimetry theory and its applications to radar detection will be given in chapter III.

2. Wave Reflections from Smooth Flat Surfaces

Using a plane incident wave to illustrate smooth surface reflection, the reflected wave is also a plane wave and this is known as specular reflection. The electric field of the reflected wave will depend on the polarization of the incident wave. It is convenient to assume that the incident wave has two components, as before. One component, $E_{iV,}$ is the "vertically" polarized component and the other, E_{iH} is the "horizontally" polarized component. This is illustrated as follows.
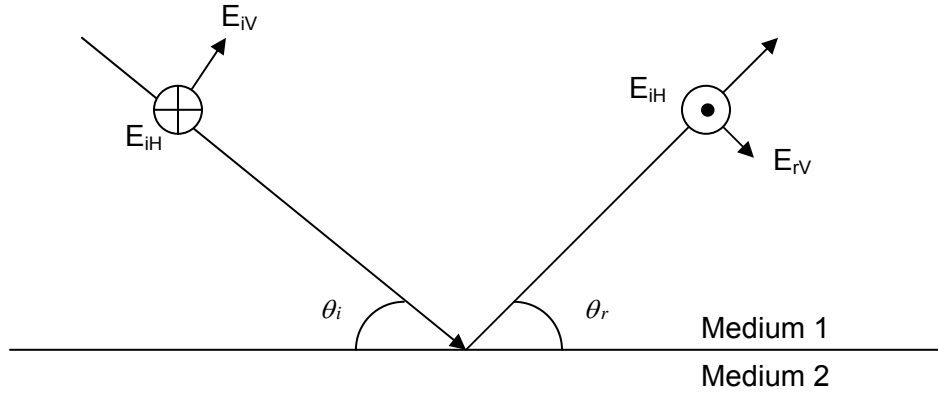
Figure II-5 Plane wave Reflection from a Smooth surface (parallel polarization)

The reflected components are related as follows [13]

$$E_{rV} = \Gamma_V E_{iV}$$

(2.24)

$$E_{rH} = \Gamma_H E_{iH}$$

where Γ is the reflection coefficient and depends on polarization of the incident wave. The polarization of the incident wave will have components parallel or perpendicular to the plane of incidence and it is convenient to express the associated reflection coefficients separately as $\Gamma_{//}$ and $\Gamma_{\perp}$. These coefficients are defined as

13

$$\Gamma_{//} = \frac{H_r}{H_i} = \frac{\eta_2 \cos\theta_t - \eta_1 \cos\theta_i}{\eta_2 \cos\theta_t + \eta_1 \cos\theta_i}$$

$$\Gamma_\perp = \frac{E_r}{E_i} = \frac{\eta_2 \cos\theta_i - \eta_1 \cos\theta_t}{\eta_2 \cos\theta_i + \eta_1 \cos\theta t}$$

(2.25)

where η is the intrinsic impedance. This expression shows clearly the dependence of wave reflection on material properties and wave polarization.

3.   Composite Reflections

For smooth but irregular surfaces, each part of the incident wave corresponds to reflections in different directions. As a result a divergence factor D, suggested by Kerr (1964) [13], needs to be included in the derivation of the reflected E-field.

In the case of a rough surface, the irregularities can be thought of as fluctuations about an "average" flat value and such surfaces can still reflect waves in a specular manner. Rough surfaces can be modeled by assuming a Gaussian variation of surface height and have a roughness (loss coefficient) of [13],

$$\rho_s = \exp\left[-8\left(\frac{\pi h_{rms}}{\lambda}\right)^2 \sin^2\theta\right]$$

(2.26)

where h_{rms} is the standard deviation of the height variations about the average flat surface and θ is the incident angle.

By combining results of the preceding sections, we may determine magnitude and phases of the reflected fields when reflections occur from a rough spherical surface, as [13]:

$$E_{rV} = \Gamma_V D \rho_s E_{iV}$$

(2.27)

$$E_{rH} = \Gamma_H D \rho_s E_{iH}$$

C.   RADAR CROSS SECTION (RCS) σ

The radar cross section is the portion of the back-scattered power corresponding to the particular polarization of the receiving antenna. Thus,

$$\sigma = \lim_{R \to \infty} 4\pi R^2 \frac{\left\{ \begin{array}{l} power\ per\ unit\ area\ in\ scattered \\ wave\ at\ receiving\ antenna \\ which\ is\ in\ the\ polarization\ of \\ receiving\ antenna \end{array} \right\}}{\left\{ \begin{array}{l} power\ per\ unit\ area\ in \\ wave\ incident\ on\ target \end{array} \right\}}$$

This definition implies that only the portion of the scattered wave at the receiving antenna that has the same polarization of the antenna is used in defining σ. Since the receiving antenna may have any specified polarization, the definition of σ of any arbitrarily polarized scattered wave should be divided into two parts – one to which the radar responds and the other that is orthogonal to the first.

We define the E-field scattered by the target and returning to the receiving antenna (in cylindrical coordinates) by the sum of components

$$E_S = E_\theta \hat{\theta} + E_\phi \hat{\phi} = \begin{bmatrix} E_\theta \\ E_\phi \end{bmatrix} \tag{2.28}$$

Figure II-6 gives the geometrical relation between the target and the receiver and the definitions of the various parameters.
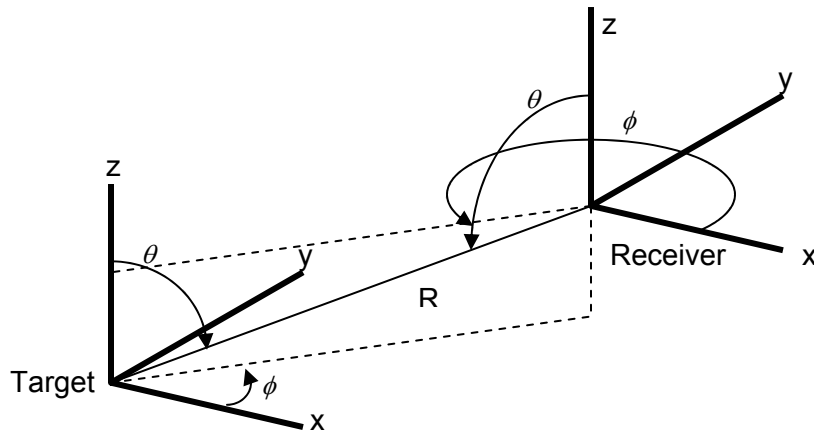
Figure II-6 Scattering Geometry

15

Using matrix notation and defining Q as the polarization ratio [13], which carries the polarization information of the EM wave and is analogous to P for the case of plane waves,

$$Q = \frac{E_\phi}{E_\theta}$$
(2.29)

the E-field becomes,

$$E_S = E_\theta \begin{bmatrix} 1 \\ Q \end{bmatrix}$$
(2.30)

Next we define the scattered E-field, E_s as a composition of polarized states, E_A, having an arbitrary but specified polarization and, E_B that is orthogonal to E_A. These components are represented as [13]

$$E_A = A_1\hat{\theta} + A_1 Q_A \hat{\phi} = A_1 \begin{bmatrix} 1 \\ Q_A \end{bmatrix}$$

$$E_B = A_2\hat{\theta} + A_3\hat{\phi} = \begin{bmatrix} A_2 \\ A_3 \end{bmatrix}$$
(2.31)

$$E_S = E_A + E_B$$

where A_1, A_2 and A_3 are parameters to be defined so that the above is true, and $A_1 \neq 0$ is assumed. Q_A is the polarization ratio based on the polarization of the receiving antenna. Since E_A is orthogonal to E_B, the following condition must be satisfied:

$$E_A \bullet E_B = A_1 \begin{bmatrix} 1 & Q_A \end{bmatrix} \begin{bmatrix} A_2^* \\ A_3^* \end{bmatrix} = A_1(A_2^* + Q_A A_3^*) = 0$$
(2.32)

Using equation (2.32) and (2.31) to solve for A_1, A_2 and A_3, we obtain the following expressions,

$$A_1 = \frac{E_\theta(1+Q_A^*Q)}{1+|Q_A|^2}$$

$$A_2 = \frac{-E_\theta Q_A^*(Q-Q_A)}{1+|Q_A|^2} \qquad (2.33)$$

$$A_3 = \frac{E_\theta(Q-Q_A)}{1+|Q_A|^2}$$

This result shows that any arbitrarily backscattered wave can be decomposed into the sum of 2 waves, E_A and its orthogonal component E_B, to which the receiving antenna can respond. The power density in the wave component E_A, which will be received by the antenna is then,

$$\text{Power density in } E_A = \frac{|E_A|^2}{2\eta} = \frac{|E_\theta|^2 |1+Q_A^*Q|^2}{2\eta(1+|Q_A|^2)} \qquad (2.34)$$

We can express σ in terms of the polarization ratios and as a function of the total scattered RCS, σ_s.

$$\sigma_s = \lim_{R_2\to\infty} 4\pi R^2 \frac{|E_s|^2}{|E_i|^2} = \lim_{R_2\to\infty} 4\pi R^2 \frac{|E_\theta|^2}{|E_i|^2}(1+|Q|^2)$$

$$\qquad (2.35)$$

$$\sigma = \lim_{R_2\to\infty} 4\pi R^2 \frac{|E_A|^2}{|E_i|^2} = \lim_{R_2\to\infty} 4\pi R^2 \frac{|E_\theta|^2}{|E_i|^2} \frac{|1+Q_A^*Q|^2}{(1+|Q_A|^2)}$$

Finally, we obtain,

$$\sigma = \sigma_s \rho_{pol}$$

$$\qquad (2.36)$$

$$\rho_{pol} = \frac{|1+Q_A^*Q|^2}{(1+|Q_A|^2)(1+|Q|^2)}$$

17

ρ_{pol} is known as the polarization efficiency or polarization match factor [11], having a range of $0 < \rho_{pol} < 1$. The polarization match factor shows how well a receiving antenna is matched in polarization to an incoming wave. It can be used to study scenarios whereby the polarizations of the transmitting and the receiving antennas are different.

D.   THE RADAR SYSTEM

This section will describe the operation of a radar system using some of the aforementioned theories.

1.   The Radar Signal Waveform

Similar to the EM wave, the radar signal waveform takes the form of a time-varying sinusoidal wave that may be represented as [10],

$$s(t) = a(t)\cos[\omega_0 t + \theta(t) + \phi_0] \qquad (2.37)$$

where a gives the amplitude, $\theta(t)$ is the phase term, ϕ_0 is a arbitrary phase angle and ω_0 is the carrier frequency. Usually, the carrier frequency is removed before signal processing. Hence, amplitude, phase and frequency modulation are directly related to these parameters. The (modulus of the) Fourier transform of the radar signal gives the spectrum of the signal.

The signal waveform is often defined over the time interval for which the radar signal is pulsed. A pulse train of waveforms is illustrated in Figure II-7, with the pulse width and the pulse repetition interval (PRI) defined graphically.
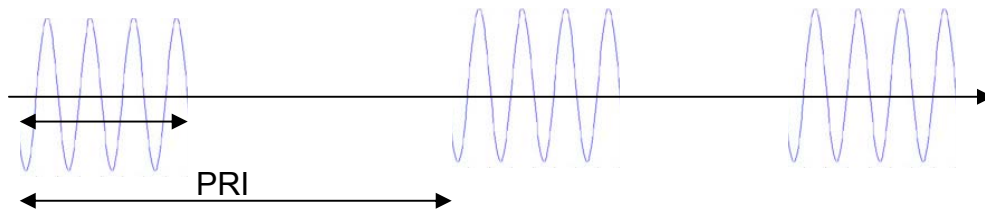
Figure II-7 Pulse train

The average peak transmitted power is given by,

$$P_t = \frac{\langle a^2(t) \rangle}{2} \tag{2.38}$$

The average power is then,

$$P_{av} = \frac{\tau}{T} P_t \tag{2.39}$$

where τ is the pulse duration and T is the integration time.

2.   Radar Equation [10]

The power transmitted by the radar antenna is first assumed to be radiated spherically, and the power density at a distance R from the radar is then,

$$\frac{P_t}{4\pi R^2} \tag{2.40}$$

where P_t is the power output by the transmitting antenna.

Taking into consideration a directional antenna in order to increase power density in a certain direction, the power density is multiplied by a directive gain, G that is usually a scalar function of the direction angles.

$$\frac{P_t G}{4\pi R^2} \tag{2.41}$$

The radiated power is then incident on the target and the reflected amount is determined by the RCS, σ. The reflected power is re-radiated spherically from the target and σ behaves like an "antenna gain".

$$\frac{P_t G}{4\pi R^2} \cdot \frac{\sigma}{4\pi R^2} \tag{2.42}$$

The reflected power is then intercepted by the radar antenna, with effective area $A_e = \dfrac{G\lambda^2}{4\pi}$, and so the final power received is,

$$P_t = \frac{P_t G \sigma}{(4\pi R^2)^2} A_e = \frac{P_t G^2 \lambda^2 \sigma}{(4\pi)^3 R^4} \tag{2.43}$$

In practical situations, the returned signals received by the radar will be corrupted by thermal noise,

$$N_i = kTB \qquad (2.44)$$

where k is the Boltzman's constant, T is the effective temperature and B is the bandwidth (equal to $1/\tau$). In order to derive the Signal-to-Noise-Ratio (SNR), we let the power received be the minimum detectable signal by the radar, S_{min}. The quantities S_{min}, N_i and SNR are related by a radar figure of merit, F, the noise figure.

$$S_{min} = kTBF(SNR) \qquad (2.45)$$

Finally, the radar equation describing the SNR becomes,

$$(SNR) = \frac{P_t G^2 \lambda^2 \sigma}{(4\pi)^3 kTBFLR^4} \qquad (2.46)$$

where L denotes the radar losses [10].

III.   POLARIMETRY THEORY

A.   JONES VECTOR

The Jones vector is introduced as a matrix representation of the polarization state of the electric field. The Jones vector that represents a polarization state can be decomposed into any orthogonal polarization basis.

Using the definitions in equation (2.15), a propagating EM wave E(z) is represented as a sum of its components in the x and y directions. Because these components oscillate with the same frequency for the monochromatic case, we can suppress the temporal term, exp($j\omega t$) and the equation becomes,

$$E(z) = e^{-jkz} \begin{bmatrix} |E_x| e^{j\delta_x} \\ |E_y| e^{j\delta_y} \end{bmatrix} \tag{3.1}$$

Furthermore, as the wave is planar, the magnitude of the electric field E(z) is the same at every point of its propagation. Hence we may set z=0 for convenience and the equation is further reduced to,

$$E(0) = E_0 = \begin{bmatrix} |E_{0x}| e^{j\delta_x} \\ |E_{oy}| e^{j\delta_y} \end{bmatrix} \tag{3.2}$$

The vector E(0) is called the Jones vector of the wave. The amplitude and phase of the complex components of the electric field are completely defined by this vector.

1.   Ellipticity Definitions

Once again, we can define the phase difference between the components of the field as $\delta = \delta_y - \delta_x$. Then from the Jones vector, we can determine the information necessary to construct the polarization ellipse [8].

The tilt φ is

$$\tan 2\varphi = \frac{2\,|\,E_x\,|}{|\,E_x\,|^2 - |\,E_y\,|^2}\cos\delta \qquad (3.3)$$

The ellipticity τ is

$$\sin 2\tau = \frac{2\,|E_x|\,|E_y|}{|E_x|^2 + |E_y|^2}\sin\delta \qquad (3.4)$$

The magnitude of the wave is

$$E_0 = \sqrt{|\,E_x\,|^2 + |\,E_y\,|^2} \qquad (3.5)$$

Conversely, the Jones vector can also be derived from the polarization ellipse using the general equation

$$E_{(x,y)} = Ae^{-j\delta}\begin{bmatrix} \cos\varphi & -\sin\varphi \\ \sin\varphi & \cos\varphi \end{bmatrix}\begin{bmatrix} \cos\tau \\ j\sin\tau \end{bmatrix} \qquad (3.6)$$

2.   Polarization States

The Jones vector conveniently describes many different polarization states – especially when further simplification is performed. The phase δ_x is set to zero as a reference, so that $\delta_y = \delta$. Then the Jones vector can be expressed in the form [12]:

$$E_0 = \begin{bmatrix} E_{0x} \\ E_{0y}e^{j\delta} \end{bmatrix} = \begin{bmatrix} A \\ be^{i\delta} \end{bmatrix} \qquad (3.7)$$

Using Euler's formula we write
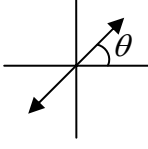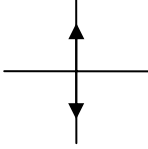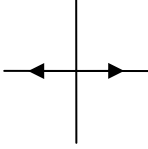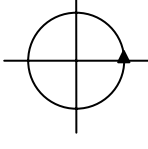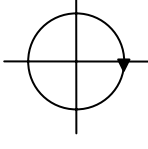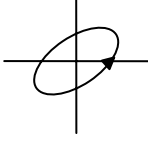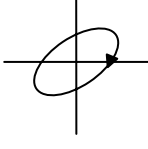
$$be^{i\delta} = b(\cos\delta + j\sin\delta) = B + iC \qquad (3.8)$$

so that the Jones vector for this case is

$$E_0 = \begin{bmatrix} A \\ B + jC \end{bmatrix} \qquad (3.9)$$

22

This form of the Jones vector is completely general and represents all polarization states through variations of the parameters A, B and C. A normalized form exists whereby the Jones vector is divided by $\sqrt{A^2 + B^2 + C^2}$.

Table III-1: Jones Vectors for Some General Polarization States [12]

General Linear Polarization	$E_0 = \begin{bmatrix} \cos\theta \\ \sin\theta \end{bmatrix}$	
Vertical Linear Polarization	$E_0 = \begin{bmatrix} 0 \\ 1 \end{bmatrix}$	
Horizontal Linear Polarization	$E_0 = \begin{bmatrix} 1 \\ 0 \end{bmatrix}$	
Left Circular Polarization	$E_0 = \frac{1}{\sqrt{2}} \begin{bmatrix} 1 \\ j \end{bmatrix}$	
Right Circular Polarization	$E_0 = \frac{1}{\sqrt{2}} \begin{bmatrix} 1 \\ -j \end{bmatrix}$	
Left Elliptical Polarization	$E_0 = \frac{1}{\sqrt{A^2 + B^2 + C^2}} \begin{bmatrix} A \\ B + jC \end{bmatrix}$	
Right Elliptical Polarization	$E_0 = \frac{1}{\sqrt{A^2 + B^2 + C^2}} \begin{bmatrix} A \\ B - jC \end{bmatrix}$	

B.   PARTIAL POLARIZATION AND STOKES VECTOR

So far, we have considered only monochromatic waves that are completely polarized and in which the other wave attributes (amplitude and phase) are time invariant. A discussion of partial polarization is included here for completeness and to illustrate the usefulness of Stokes vectors representations.

By partial polarization, we mean a quasi-monochromatic wave with time-dependent amplitude and phase. The wave polarization traces an ellipse with time-varying tilt and amplitude. As further illustration, Mott [11] characterized a quasi-monochromatic wave to be a sum of a completely polarized and a completely unpolarized wave from which the degree of polarization can be defined.

1.   Coherency Matrix

Using this decomposition concept, and because of the time-variant or stochastic nature of partially polarized waves, a coherency matrix containing the correlations between polarized and unpolarized components of the electric field is used. The derivation of the coherency matrix (as detailed in [2] and [11]) can be visualized through geometric optics because, optically, coherency is the ability to form interference fringes [2]. Recalling the definition of the E-field from (2.12), $E = \mathrm{Re}[E_0 e^{j(\omega t - kz)}]$ and propagating this E-field through a bire-fringent phase plate that introduces a phase difference δ between the x and y components, we may re-write the field as one propagating along the z-axis and making an angle θ to the x-axis, so that:

$$E_0(t,\theta) = E_x \cos\theta + E_y e^{j\delta} \sin\theta \qquad (3.10)$$
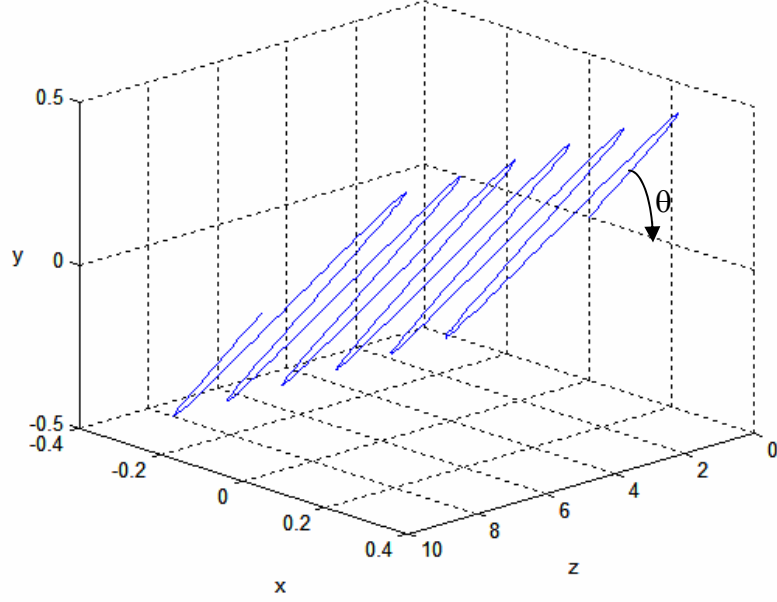
Figure III-1 Illustration of Wave Propagating in z-direction

The time-averaged intensity is then:

$$<|E_0|^2> = J_{xx}\cos^2\theta + J_{yy}\sin^2\theta + (J_{xy}e^{-j\delta} + J_{yx}e^{j\delta})\cos\theta\sin\theta \quad (3.11)$$

where [J] is the coherency matrix and the elements are averaged over a number of oscillations or cycles as denoted by the angular brackets:

$$[J] = \begin{bmatrix} J_{xx} & J_{xy} \\ J_{yx} & J_{yy} \end{bmatrix} = \begin{bmatrix} \langle E_x(t)E_x^*(t) \rangle & \langle E_x(t)E_y^*(t) \rangle \\ \langle E_x^*(t)E_y(t) \rangle & \langle E_y(t)E_y^*(t) \rangle \end{bmatrix} \quad (3.12)$$

Unpolarized waves have time averages that are independent of the angle the wave makes to the x-y axis as it propagates along the z-direction; i.e., over time, the amplitude of the power or time-averaged intensity does not depend on the polarization of the E-field since the E-field has no constant polarization state. This requires that:

$$J_{xx} = J_{yy} \quad (3.13)$$

$$J_{xy} = 0 = J_{yx} \quad (3.14)$$

The coherency matrix is important in partial polarization: its trace, determinant and eigenvalues all have a direct mathematical relationship to the

25

degree of polarization, P. The coherency matrix can also be subjected to unitary transform so that it can be decomposed into its unpolarized and polarized components. However, the coherency matrix is difficult to visualize and, alternatively, Stokes vectors can be used to characterize the amplitude and polarization of partially polarized waves.

2.   Stokes Vector

For completely polarized or monochromatic waves, the Stokes vectors are introduced simply as [11]:

$$S_0 = |E_x|^2 + |E_y|^2 \tag{3.15}$$

$$S_1 = |E_x|^2 - |E_y|^2 \tag{3.16}$$

$$S_2 = 2|E_x||E_y|\cos\delta \tag{3.17}$$

$$S_3 = 2|E_x||E_y|\sin\delta \tag{3.18}$$

where E and δ are as previously defined. It can be seen that from the Stokes vectors, all information about the amplitude and polarization can be defined. In particular, note also that:

$$S_o^2 = S_1^2 + S_2^2 + S_3^2 \tag{3.19}$$

The Stokes vector is often expressed in matrix form as:

$$S = \begin{bmatrix} S_0 \\ S_1 \\ S_2 \\ S_3 \end{bmatrix} \tag{3.20}$$

We can also relate the Stokes vectors to the polarization ellipse parameters:

$$\tan 2\varphi = \frac{2|E_x|}{|E_x|^2 - |E_y|^2}\cos\delta = \frac{S_2}{S_1} \tag{3.21}$$

26

$$\sin 2\tau = \frac{2|E_x||E_y|}{|E_x|^2 + |E_y|^2} \sin \delta = \frac{S_3}{S_0} \qquad (3.22)$$

In the partially polarized case, we separate the Stokes vectors into the polarized and unpolarized components as before,

$$S = \begin{bmatrix} S_0 \\ S_1 \\ S_2 \\ S_3 \end{bmatrix}_{pol} + \begin{bmatrix} S_0 \\ S_1 \\ S_2 \\ S_3 \end{bmatrix}_{unpol} \qquad (3.23)$$

With some manipulation we establish the relationship between the coherency matrix and the Stokes vector.

$$S_0 = J_{xx} + J_{yy} \qquad (3.24)$$

$$S_1 = J_{xx} - J_{yy} \qquad (3.25)$$

$$S_2 = J_{xy} + J_{yx} \qquad (3.26)$$

$$S_3 = j(J_{xy} - J_{yx}) \qquad (3.27)$$

Then for the completely unpolarized case, from (3.13) and (3.14), we have

$$S_1 = S_2 = S_3 = 0 \qquad (3.28)$$

and,

$$S = \begin{bmatrix} RS_0 \\ S_1 \\ S_2 \\ S_3 \end{bmatrix} + \begin{bmatrix} (1-R)S_0 \\ 0 \\ 0 \\ 0 \end{bmatrix} \qquad (3.29)$$

where R is the degree of polarization and can be defined as:

$$R = \frac{S_{0pol}}{S_0} = \frac{\sqrt{S_1^2 + S_2^2 + S_3^2}}{S_0} = \sqrt{1 - \frac{4\det\{[J]\}}{(J_{xx} + J_{yy})^2}} \qquad (3.30)$$

Note that for the completely polarized case, R=1 and the equation reduces back to (3.20).

3.   Poincarē Sphere

The Poincarē sphere is a geometrical visualization of the Stokes vectors. Re-expressing the Stokes vectors in terms of S_0, φ and τ (from the polarization ellipse), we obtain [11]:

$$S_1 = S_0 \cos 2\tau \cos 2\varphi \tag{3.31}$$

$$S_2 = S_0 \cos 2\tau \sin 2\varphi \tag{3.32}$$

$$S_3 = S_0 \sin 2\tau \tag{3.33}$$

It is then apparent that S_1, S_2 and S_3 are the Cartesian coordinates of a point on a sphere with radius S_0. 2φ and 2τ are the azimuthal and elevation angles respectively. It is also popular to express the Stokes vectors in terms of the Deschamps parameters that are mathematically defined as [8]:

$$\begin{pmatrix} S_1 \\ S_2 \\ S_3 \end{pmatrix} = S_0 \begin{pmatrix} \cos 2\gamma \\ \sin 2\gamma \cos 2\varepsilon \\ \sin 2\gamma \sin 2\varepsilon \end{pmatrix} \tag{3.34}$$

Hence, any polarization state can be described by a point on the sphere and vice versa.

28
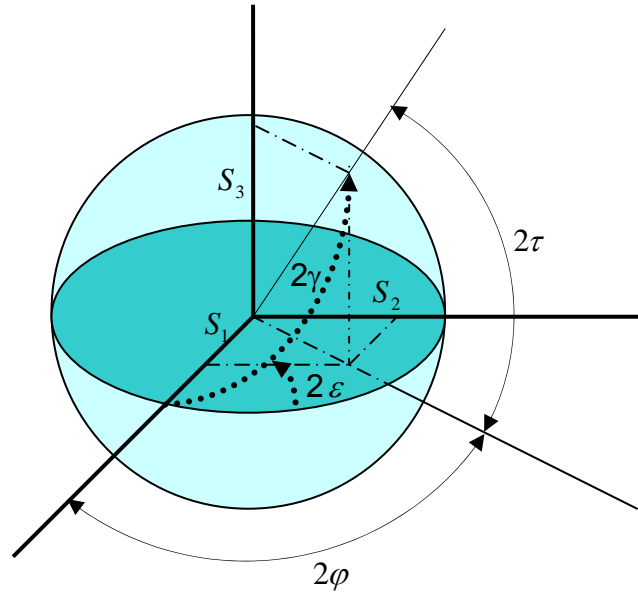
Figure III-2 Poincarē sphere[11]

In addition to the Stoke's vectors, the Poincarē sphere also carries information about the p, q and P (the various polarization ratios defined in Chapter II) that can be visualized on the sphere itself. This is done by mapping the Poincarē sphere onto the complex plane. Before doing so, we summarize the parameters for some cases of polarizations.

Table III-2 Polarization Parameters for Some Polarization States [11]

Polarization	p	P	q	S_1	S_2	S_3
Right Circular	1	-j	0	0	0	$-S_0$
Left Circular	-1	j	∞	0	0	S_0
Linear Vertical	$j\infty$	∞	-1	S_0	0	0
Linear Horizontal	0	0	1	1	S_0	0

Figure III-3 shows the way to map a point on the Poincarē sphere onto the p, P complex planes to obtain their values. The north-pole (z-axis) of the sphere is aligned with the real axis of the p plane and the equator of the sphere is aligned with the imaginary axis. The mapping is done by drawing a line that intersects (i) the furthest point on the sphere from the plane (specifically the

highest point along the x-axis in this illustration), (ii) the point of interest in the sphere and (iii) the projection point on the p complex plane.

In Figure III-3, point A, which is also the north pole of the sphere, describes p=-1 and P= j, which is a projection from the point (0, 0, S_0) of the sphere (with Cartesian coordinates (S_1, S_2, S_3)). Point B describes p=j and P=1, which is projected from the point (0, S_0, 0) from the sphere. This construction agrees with Table III-2. Any other point on the sphere referring to any polarization states can be mapped in a similar manner.
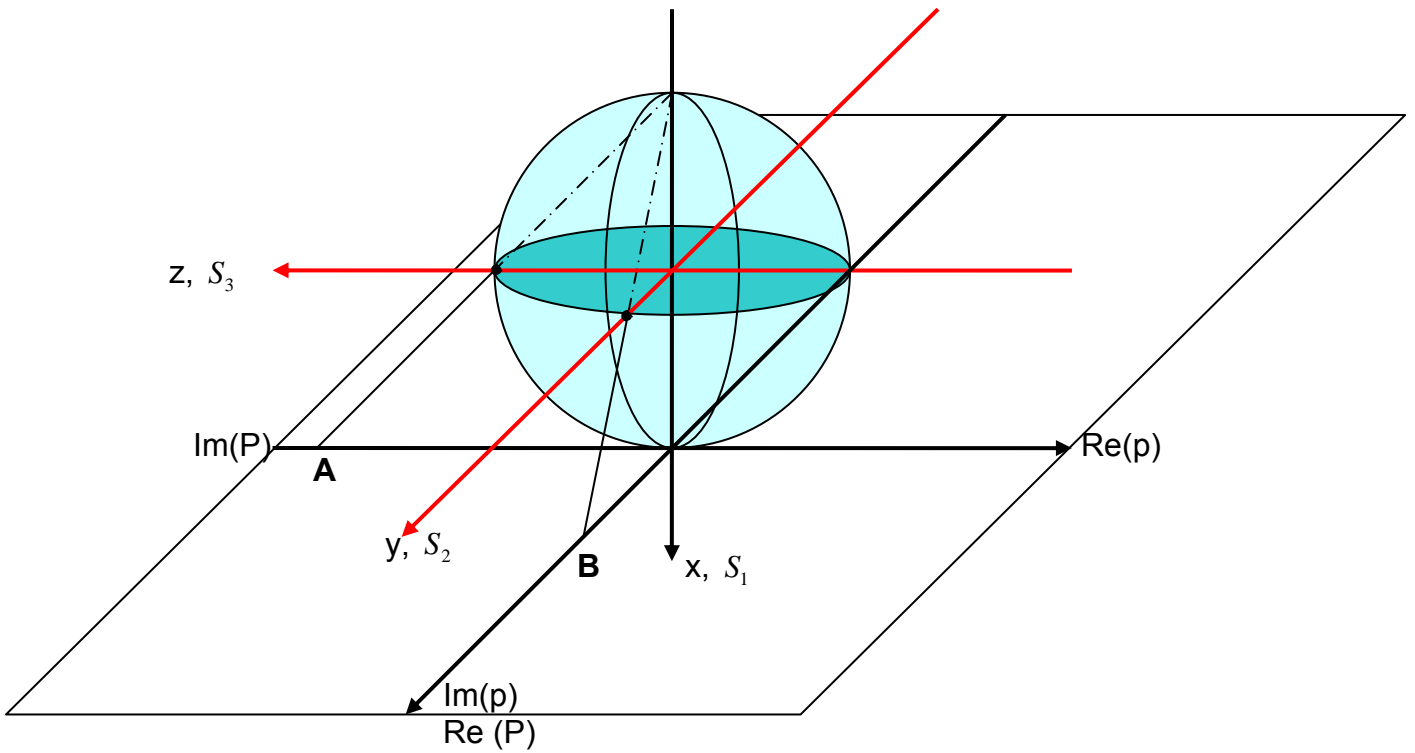
Figure III-3 Mapping of Poincarē sphere onto p and P Complex Plane [11]

C.   SCATTERING/ SINCLAIR MATRIX

When an EM wave is incident on a target, the polarization of the back-scattered wave is generally different from the incident wave and the geometry of the target will determine the extent of depolarization. Sinclair proved that the

30

target acts as a polarization transformer and defined this change by a 2 x 2 scattering matrix [8].

$$[A] = \begin{bmatrix} A_{xx} & A_{xy} \\ A_{yx} & A_{yy} \end{bmatrix}$$

(3.35)

The important concept of the scattering matrix is that it links the two orthogonal components of the incident Jones vector to the back-scattered components.

$$\begin{bmatrix} E_x^r \\ E_y^r \end{bmatrix} = \frac{1}{\sqrt{4\pi r}} \begin{bmatrix} A_{xx} & A_{xy} \\ A_{yx} & A_{yy} \end{bmatrix} \begin{bmatrix} E_x^i \\ E_y^i \end{bmatrix}$$

(3.36)

The distance term $\dfrac{1}{\sqrt{4\pi r}}$ is often omitted from literature since only the polarization is of interest most of the time. For a mono-static system (where the radar transmitter and receiver are co-located), the reciprocity theorem[1] states that the cross polarization terms are equal [9].
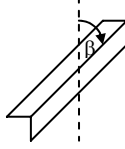
$$A_{xy} = A_{yx}$$

(3.37)

1.   Examples of Scattering Matrices of Canonical Targets

The scattering matrices are dependent on the geometry of the targets. Once the scattering matrix is specified, the back scattered wave can be computed for any incident wave polarization state. The scattering matrices of a number of canonical targets have been well established in literature and are tabulated here.

---

[1] Reciprocity Theorem - If a voltage source E acting in one branch of a network causes a current I to flow in another branch of the network, then the same voltage source E acting in the second branch would cause an identical current I to flow in the first branch.

Table III-3 Scattering Matrices of some Canonical Targets [8],[2]

Rectangular Flat Plat or Sphere	$A_{plate} = \begin{bmatrix} 1 & 0 \\ 0 & 1 \end{bmatrix}$	
Dihedral	$A_{dihedral} = \begin{bmatrix} \cos 2\beta & \sin 2\beta \\ \sin 2\beta & -\cos 2\beta \end{bmatrix}$	
Metallic Helix	$A_{helix} = \frac{1}{2}\begin{bmatrix} 1 & -j \\ -j & -1 \end{bmatrix}$	

2. Determination and Measurement of the Scattering Matrix

The scattering matrix contains all the information about the scattering properties of the target. The elements of the scattering matrix are generally complex quantities that may be expressed as [14]

$$[A] = \begin{bmatrix} |A_{xx}|e^{i\phi_{xx}} & |A_{xy}|e^{i\phi_{xy}} \\ |A_{yx}|e^{i\phi_{yx}} & |A_{yy}|e^{i\phi_{yy}} \end{bmatrix} \tag{3.38}$$

The components of the matrix are related to the scattering cross section by

$$\sigma_{xx} = 4\pi r^2 |A_{xx}|^2, \quad \sigma_{xy} = 4\pi r^2 |A_{xy}|^2$$
$$\sigma_{yx} = 4\pi r^2 |A_{yx}|^2, \quad \sigma_{yy} = 4\pi r^2 |A_{yy}|^2 \tag{3.39}$$

where r is the range of the target. Hence the specification of the scattering matrix is dependent on the measurement of the scattering cross section of the target. In the mono-static case $A_{xy} = A_{yx}$, and this leaves three amplitudes and three phases to evaluate. The absolute phase depends on the distance of the target to the radar and the target orientation. It is almost impossible to measure the

32

absolute phase accurately and a relative phase measurement is used instead. In this case, one of the phase terms, e.g., ϕ_{xx}, is factored out and the scattering matrix becomes

$$[S] = e^{i\phi_{xx}} \begin{bmatrix} \sqrt{\sigma_{xx}} & \sqrt{\sigma_{xy}}\, e^{i(\phi_{xy}-\phi_{xx})} \\ \sqrt{\sigma_{yx}}\, e^{i(\phi_{yx}-\phi_{xx})} & \sqrt{\sigma_{yy}}\, e^{i(\phi_{yy}-\phi_{xx})} \end{bmatrix} \frac{1}{\sqrt{4\pi r}} \qquad (3.40)$$

Then, five quantities are left to be measured for the monostatic case: three amplitudes and two relative phases. Relative phases are easier to measure than the absolute phase since they are not dependent on the target distance. Also, absolute phase is not necessary for most cases to determine the polarization states. Ruck et. al. [14] provides the elements to be measured in a laboratory transmit and receive scenario for both absolute and relative phase method.

3. Optimal Polarizations

We can make use of the scattering matrices and the polarization match factor or polarization ratios introduced in Chapter II to determine the polarization whereby the received power is a maximum or a minimum.

The scattering matrix in one polarization basis may be transformed to another polarization basis in a different orientation, e.g., in a bi-static scenario whereby the transmitting and the receiving antenna may not have the same polarization states. This is done using a unitary transformation matrix [4],[8]:

$$[A]_{ab} = [U][A]_{xy}[U]^T \qquad (3.41)$$

where ,

$$[U] = \begin{bmatrix} \cos\alpha & \sin\alpha\, e^{j\delta} \\ -\sin\alpha\, e^{-j\delta} & \cos\alpha \end{bmatrix} \qquad (3.42)$$

and α describes the change in orientation angle between the two polarization bases. We have previously defined the polarization ratio in (II-21) as $P = \tan\varphi\, e^{j\delta}$

relating the orthogonal components of an EM wave. It can be redefined analogously as a polarization ratio that describes the change in polarization basis as:

$$P = \tan \alpha \; e^{j\delta} \tag{3.43}$$

In this case, the unitary transformation matrix can then be written simply as:

$$[U] = \frac{1}{\sqrt{1 + PP^*}} \begin{bmatrix} 1 & P \\ -P^* & 1 \end{bmatrix} \tag{3.44}$$

Now the elements of the $[A]_{ab}$ matrix can be written as:

$$\begin{aligned}
A_{aa} &= (1 + PP^*)^{-1}[A_{xx} + P^2 A_{yy} + P(A_{xy} + A_{yx})] \\
A_{ab} &= (1 + PP^*)^{-1}[-P^* A_{xx} + P A_{yy} + A_{xy} - PP^* A_{yx})] \\
A_{ba} &= (1 + PP^*)^{-1}[-P^* A_{xx} + P A_{yy} + A_{yx} - PP^* A_{xy})] \\
A_{bb} &= (1 + PP^*)^{-1}[-P^{*2} A_{xx} + A_{yy} - P^*(A_{xy} + A_{yx})]
\end{aligned} \tag{3.45}$$

In the optimization problem, we can visualize the two scattering matrices as the transformation in polarization state when the EM wave is depolarized by a target. The power of the scattered wave is distributed into two channels of reception, the co-polarized channel (identical to the polarization state of the transmitting antenna) and the cross-polarized channel (orthogonal to the polarization state of the receiving antenna).

Figure III-4 Polarization States of Transmitted and Backscattered Waves

It was first shown by Kennaugh that there exist two pairs of optimal polarizations states [1]. The co-polarization null pair (CO-POL) for minimal co-polarization (and maximum cross-polarization) is obtained by setting A_{aa} and A_{bb} to zero so that [2]:

$$P_{1,2}^{co} = \frac{-(A_{xy} + A_{yx}) \pm \sqrt{\left(A_{xy} + A_{yx}\right)^2 - 4A_{xx}A_{yy}}}{2A_{yy}} \tag{3.46}$$

The cross polarization null pair (X-POL) for maximal polarization is obtained by setting A_{ab} and A_{ba} to zero so that [2]:

$$P_{1,2}^{x} = \frac{-R_1 \pm \sqrt{R_1^2 + 4R_2 R_3}}{2R_2}$$

$$R_1 = (|A_{yy}|^2 - |A_{xx}|^2 - A_{xy}A_{yx}^* + A_{yx}A_{xy}^*) \tag{3.47}$$

$$R_2 = (A_{yy}A_{yx}^* + A_{yx}A_{xx}^*)$$

$$R_3 = (A_{xx}A_{xy}^* + A_{xy}A_{yy}^*)$$

The CO-POL and the X-POL pairs are often plotted onto the Poincarē sphere forming what is known as the *Polarization fork*, originally conceived by Huynen.

Many optimization techniques have been developed and a good summary is found in [1]. Such techniques may involve matrix manipulation of a target scattering matrix to derive its eigenvalues, deriving the polarization ratios from the Poincare sphere or using the Stokes vector and Muller matrix. Optimization of polarization states will be further discussed in Chapter IV through its implementation in Matlab.

D.   MUELLER (POWER) MATRIX

For the partially polarized case, it is necessary to relate the incident and scattered Stokes vector. Just as the incident and scattered Jones vector is related by the scattering matrix, the incident and scattered Stokes vector is related by the Mueller matrix [8]:

$$S_{scattered} = [M]S_{incident} \tag{3.48}$$

We express the Stokes vector in the energy form to give [9]:

$$S = \begin{bmatrix} 1 & 1 & 0 & 0 \\ 1 & -1 & 0 & 0 \\ 0 & 0 & 1 & 1 \\ 0 & 0 & -j & -j \end{bmatrix} \begin{bmatrix} |E_x|^2 \\ |E_y|^2 \\ E_x E_y^* \\ E_y E_x^* \end{bmatrix} \qquad (3.49)$$

Then relation between the incident and scattered energy is given by the relation

$$\begin{bmatrix} |E_x^s|^2 \\ |E_y^s|^2 \\ E_x^s E_y^{s*} \\ E_x^s E_x^{s*} \end{bmatrix} = [A \otimes A^*] \begin{bmatrix} |E_x^i|^2 \\ |E_y^i|^2 \\ E_x^i E_y^{i*} \\ E_x^i E_x^{i*} \end{bmatrix} \qquad (3.50)$$

so that [14],

S^s

$$= \begin{bmatrix} 1 & 1 & 0 & 0 \\ 1 & -1 & 0 & 0 \\ 0 & 0 & 1 & 1 \\ 0 & 0 & -j & -j \end{bmatrix} \begin{bmatrix} A_{xx}A_{xx}^* & A_{xy}A_{yx}^* & A_{xx}A_{xy}^* & A_{xy}A_{xx}^* \\ A_{yx}A_{yx}^* & A_{yy}A_{yy}^* & A_{yx}A_{yy}^* & A_{yy}A_{yx}^* \\ A_{xx}A_{yx}^* & A_{xy}A_{yy}^* & A_{xx}A_{yy}^* & A_{xy}A_{yx}^* \\ A_{yx}A_{xx}^* & A_{yy}A_{xy}^* & A_{yx}A_{xy}^* & A_{yy}A_{xx}^* \end{bmatrix} \begin{bmatrix} 1 & 1 & 0 & 0 \\ 1 & -1 & 0 & 0 \\ 0 & 0 & 1 & 1 \\ 0 & 0 & -j & -j \end{bmatrix}^{-1} S^i$$

$$= \begin{bmatrix} M_{11} & M_{12} & 0 & 0 \\ M_{21} & M_{22} & 0 & 0 \\ 0 & 0 & M_{33} & M_{34} \\ 0 & 0 & M_{43} & M_{44} \end{bmatrix} S^i$$

(3.51)

Generally, the scattering matrix contains complex elements of a voltage and is used for coherent systems while the Mueller matrix contains power elements and is used for incoherent systems[14].

E.   TARGET DECOMPOSITION THEOREMS

Cloude [5] defines the main idea behind Target Decomposition (TD) theorems as "expressing the average scattering matrix for a random media problem as a sum of independent elements and to associate a physical mechanism with each component."

The scattering matrix is a measured quantity, often stochastic rather than deterministic in nature. The use of TD theorems to evaluate the average scattering matrix allows the various scattering mechanisms and target physical properties to be identified. In addition, it is possible to generate a dominant scattering mechanism for better physical interpretation. This is the main advantage of TD theorems.

The method described here is based on developments by Cloude and involves the use of Pauli matrices to vectorize the scattering matrix. The scattering vector can then be related to the physical attributes of the scattering target using the *Scattering Vector Reduction Theorem*. Finally, these physical attributes can be used to identify the target against a cluttered background that has different scattering mechanisms.

1.   Pauli Spin Matrices

The Pauli spin matrices (commonly used in quantum mechanics) can be used to decompose the scattering matrices. In quantum mechanics, Pauli matrices are a basis set that described microscopic particles of spin ½. Spin is a quantity similar to angular momentum in classical mechanics but is distinguished by its quantized and discrete nature [19]. The Pauli spin matrices are [9]:

$$\Psi_P = \left\{ \sqrt{2}\begin{bmatrix} 1 & 0 \\ 0 & 1 \end{bmatrix}, \sqrt{2}\begin{bmatrix} 1 & 0 \\ 0 & -1 \end{bmatrix}, \sqrt{2}\begin{bmatrix} 0 & 1 \\ 1 & 0 \end{bmatrix}, \sqrt{2}\begin{bmatrix} 0 & -j \\ j & 0 \end{bmatrix} \right\} \qquad (3.52)$$

The interpretation of the Pauli matrices is as tabulated:

Table III-4: Pauli Matrices and their Interpretation [9]

Pauli matrix	Scattering Type	Interpretation
$\begin{bmatrix} 1 & 0 \\ 0 & 1 \end{bmatrix}$	Odd- bounce	Surface, sphere, corner reflectors
$\begin{bmatrix} 1 & 0 \\ 0 & -1 \end{bmatrix}$	Even-bounce	Dihedral
$\begin{bmatrix} 0 & 1 \\ 1 & 0 \end{bmatrix}$	Even-bounce $\pi/4$ tilted	$\pi/4$ tilted dihedral, volume scattering
$\begin{bmatrix} 0 & -j \\ j & 0 \end{bmatrix}$	Cross-polariser	Non-existent for backscattering

The advantage of using a Pauli matrix basis is that the elements that result are closely related to the physics of wave scattering [4]. The scattering types that result after decomposition are orthogonal so that their separation is straightforward. As an example, recall the concept presented in Table Table III-3 that the polarization states of backscattering from targets are determined from their scattering matrices. We illustrate this again in the following Figure III-5 (notice that the two scattering matrices form two of the Pauli matrices defined above).

$$A_1 = \begin{bmatrix} 1 & 0 \\ 0 & 1 \end{bmatrix}$$

$$A_2 = \begin{bmatrix} 1 & 0 \\ 0 & -1 \end{bmatrix}$$
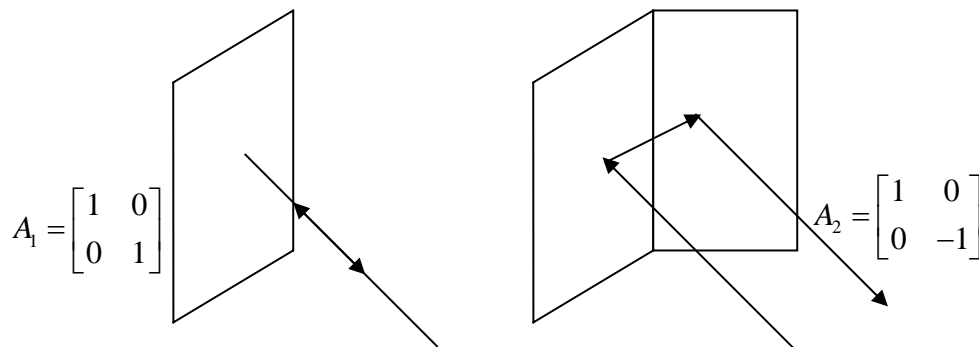
Figure III-5 Relating Scattering Matrices to Pauli Matrices

Based on this idea, the Pauli decomposition can be used to process a full polarimetric data set and separate them into their orthogonal sets. Figure III-6 of

the Great Aletsch glacier, Switzerland gives a vivid illustration of this property of the Pauli matrices [18]. Using Pauli decomposition, a three color picture of a fully polarimetric data set is constructed. Areas with even-bounce characteristics represent buildings in urban areas and are coded in red. Areas with odd-bounce characteristics representing flat surface and corner reflectors are coded in blue. Lastly areas with scattering mechanism of the third Pauli matrix that represents volume scattering are coded in green.
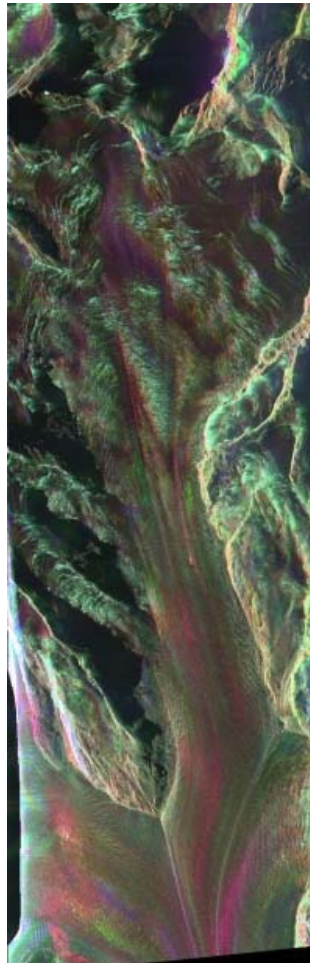
Figure III-6 Pauli Decomposition of a Full Polarimetric Data Set [9]

2.   Vectorization of Scattering Matrices

The extraction of physical information about a target involves the vectorization of its scattering matrix. The vectorization process makes use of the Pauli matrices as basis elements to separate the scattering matrix into its

physical scattering mechanism. The representation of the scattering matrix in the Pauli basis matrix results in a vector $\hat{k}$ through the following operation [5],[7]:

$$\hat{k} = \frac{1}{2} Trace([A]\Psi_P)$$

$$= \frac{1}{\sqrt{2}} Trace \left\{ \begin{bmatrix} A_{HH} & 0 \\ 0 & A_{VV} \end{bmatrix}, \begin{bmatrix} A_{HH} & 0 \\ 0 & -A_{VV} \end{bmatrix}, \begin{bmatrix} 0 & A_{HV} \\ A_{VH} & 0 \end{bmatrix}, \begin{bmatrix} 0 & jA_{HV} \\ -jA_{VH} & 0 \end{bmatrix} \right\} \quad (3.53)$$

$$= \frac{1}{\sqrt{2}} [A_{HH} + A_{VV}, A_{VV} - A_{HH}, A_{HV} + A_{VH}, j(A_{HV} - A_{VH})]^T$$

In the case of backscattering, the reciprocity theorem, as mentioned in equation(3.37), results in $A_{HV} = A_{VH}$, thereby eliminating the fourth term in the scattering vector, reducing it to:

$$\hat{k} = \frac{1}{\sqrt{2}} \begin{bmatrix} A_{HH} + A_{VV} \\ A_{VV} - A_{HH} \\ 2A_{HV} \end{bmatrix} \quad (3.54)$$

Specifically, the elements of this scattering vector are derived from a scattering matrix decomposed by a Pauli basis set. The first element $A_{HH} + A_{VV}$ is from the first Pauli matrix and hence represent an odd-bounce scattering type. The second element $A_{VV} - A_{HH}$ corresponds to an even bounce scattering type and the third element $2A_{HV}$ corresponds to the third Pauli matrix. This then illustrates how the Pauli decomposition of a full polarimetric data set is accomplished. Referring back to Figure III-6, areas coded blue are the first elements of the scattering vector, areas coded red are the second elements and areas coded green are the third elements.

In order to correlate the target scattering vector to the actual physical attribute and scattering mechanism, we need to equate the scattering vector to a general unitary complex vector [7] whose parameters are linked to physical space, so that now,

$$\hat{k} = \frac{1}{\sqrt{2}} \begin{bmatrix} A_{HH} + A_{VV} \\ A_{VV} - A_{HH} \\ 2A_{HV} \end{bmatrix} = |k|\hat{w} = |k| \begin{bmatrix} \cos\alpha \\ \sin\alpha\cos\beta \\ \sin\alpha\sin\beta \end{bmatrix} \tag{3.55}$$

Equation (3.55) may be visualized as a unitary transformation of the matrix to a different axes set (e.g. in the case of (3.36)). One way to do this is to utilize the Poincaré sphere. Hence the expression of the $\hat{k}$ vector as a unitary complex vector is analogously equivalent to rotation of the Poincaré sphere where α and β are the Deschamps parameters, previously described in (3.34) and repeated here [7]:

$$\begin{pmatrix} S_1 \\ S_2 \\ S_3 \end{pmatrix} = S_0 \begin{pmatrix} \cos 2\gamma \\ \sin 2\gamma \cos 2\varepsilon \\ \sin 2\gamma \sin 2\varepsilon \end{pmatrix} \tag{3.56}$$

To change the scattering vector $\hat{k}$ into $\hat{k}'$ with a differential change in scattering mechanism, we can introduce changes $\Delta\alpha$ and $\Delta\beta$ in the angles α and β respectively [9]. Mathematically this is done by using vector rotation algebra:

$$\hat{k}' = \begin{bmatrix} 1 & 0 & 0 \\ 0 & \cos\Delta\beta & -\sin\Delta\beta \\ 0 & \sin\Delta\beta & \cos\Delta\beta \end{bmatrix} \hat{k} \tag{3.57}$$

$$\hat{k}' = \begin{bmatrix} \cos\Delta\alpha & -\sin\Delta\alpha & 0 \\ \sin\Delta\alpha & \cos\Delta\alpha & 0 \\ 0 & 0 & 1 \end{bmatrix} \hat{k} \tag{3.58}$$

This observation leads to the important concept of the *Scattering Vector Reduction Theorem* [4] that states that "it is always possible to reduce an arbitrary scattering mechanism represented by a complex unitary vector, $\hat{k}$ to the identity $[1,0,0]^T$ by the following set of ordered matrix transformations":

$$\begin{bmatrix} 1 \\ 0 \\ 0 \end{bmatrix} = \begin{bmatrix} \cos\alpha & \sin\alpha & 0 \\ -\sin\alpha & \cos\alpha & 0 \\ 0 & 0 & 1 \end{bmatrix} \begin{bmatrix} 1 & 0 & 0 \\ 0 & \cos\beta & -\sin\beta \\ 0 & \sin\beta & \cos\beta \end{bmatrix} \hat{k} \tag{3.59}$$

We are now finally ready to interpret the above in terms of both the physical attributes of the target as well as its scattering mechanism. The two matrices above resemble the matrices for plane rotations. Physically, β corresponds to the rotation of the sensor coordinates [4]. Conversely, this angle also refers to the orientation of the target and takes on a value of -180^0 to 180^0.

The first matrix containing the angle α, though, also resembles a plane rotation and is not related to target orientation. This matrix corresponds to an internal degree of freedom of the target and hence is directly related to the type of scattering mechanism of the target [4]. The angle α is continuous within a range of 0^0 to 90^0 and can be used to represent a variety of different scatterers.
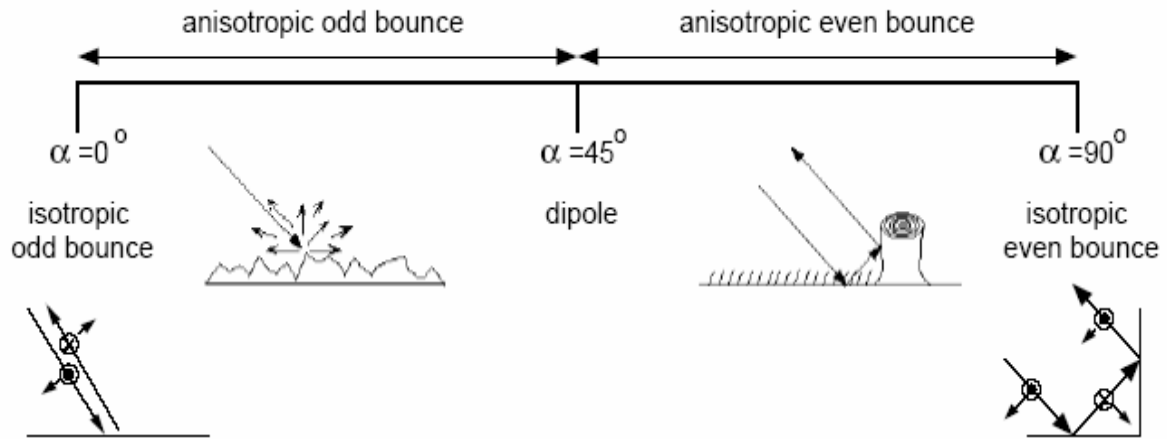
Figure III-7 Interpretation of the α angle [9]

The interpretation of the α angle is proposed and developed by Cloude [6]. He suggests that the scattering by a media can be modeled by a single dominant matrix, the coherency matrix, defined as

$$[T] = \hat{k} \cdot \hat{k}^{*T} \tag{3.60}$$

The coherency matrix $[T]$ has three eigenvalues, λ_1, λ_2 and λ_3, and the *entropy, H,* of these eigenvalues is a measure for the randomness of the averaged polarimetry scattering with H = 0 indicating a single scattering mechanism and H = 1 representing a random mixture of scattering mechanisms,

42

i.e. a depolarizing target. Values between 0 and 1 indicate the degree of dominance of one particular scatterer:

$$H = \sum_{i=1}^{3} -P_i \log_n P_i \qquad (3.61)$$

$$P_i = \frac{\lambda_i}{\sum_{j=1}^{n} \lambda_j} \qquad (3.62)$$

The angle α can be determined by the parameterization of $[T]$

$$[T] = [U_3] \begin{bmatrix} \lambda_1 & 0 & 0 \\ 0 & \lambda_2 & 0 \\ 0 & 0 & \lambda_3 \end{bmatrix} [U_3]^{*T} \qquad (3.63)$$

where

$$[U_3] = \begin{bmatrix} \cos\alpha_1 & \cos\alpha_2 & \cos\alpha_3 \\ \sin\alpha_1 \cos\beta_1 e^{j\delta_1} & \sin\alpha_2 \cos\beta_2 e^{j\delta_2} & \sin\alpha_3 \cos\beta_3 e^{j\delta_3} \\ \sin\alpha_1 \sin\beta_1 e^{j\gamma_1} & \sin\alpha_2 \cos\beta_2 e^{j\gamma_2} & \sin\alpha_3 \cos\beta_3 e^{j\gamma_3} \end{bmatrix} \qquad (3.64)$$

and

$$\alpha = P_1 \alpha_1 + P_2 \alpha_2 + P_3 \alpha_3 \qquad (3.65)$$

An $\alpha - H$ plot can be constructed that defines 9 regions for different scattering zones at different entropies (ranging from Low Entropy Surface Scattering to High Entropy Multiple Scattering).
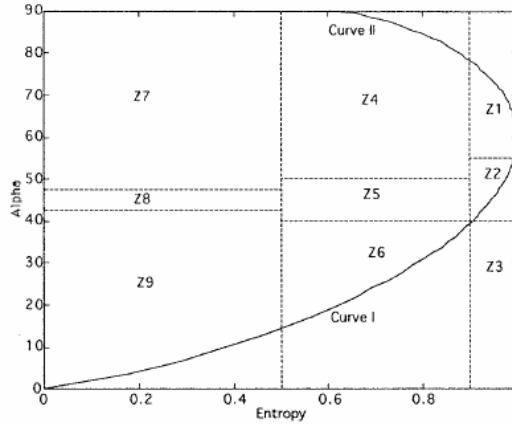
Figure III-8 Zones in α-H plane for Random Media Scattering Problems [6]

At $\alpha = 0^0$, we have an isotropic surface represented by the first Pauli matrix. As α increases, the surface becomes increasingly anisotropic. At $\alpha = 90^0$, we obtain the second Pauli matrix. This point can also be used to represent targets that cause a phase shift of 2π between the H and V components of the electric field. For intermediate values of α, the scattering mechanism becomes anisotropic and A_{HH} and A_{VV} are no longer equal. The anisotropic behaviour and consequently the increasingly different co-polar scattering coefficients means a preferential scattering in a particular direction. At the limit of $\alpha = 45^0$, this leads to a dipole scatterer whose orientation is determined by the angle β and one of the copolarized coefficient goes to zero.

The α angle is decoupled from the β angle so that scattering mechanism can be identified independently of the target's physical orientation. A list of the possible α and β angles are tabulated and mathematical examples of their derivation are given in Chapter IV.

Table III-5 Examples of α and β angles for Canonical Targets [9]

Canonical Scatterer	α	β
Sphere	0^0	-180^0 to180^0
Dihedral at θ	90^0	2θ
Dipole at θ	45^0	2θ
Helix	90^0	$\pm45^0$
Surface at θ	0^0	2θ

Many other TD theorems exist and different approaches seek to extract different information. The TD theorems may also be applied to the various polarization matrices besides the scattering matrix such as the coherence and the Mueller matrices. A good review of the various approaches is available in [5] and [9], pg 43-58.

THIS PAGE INTENTIONALLY LEFT BLANK

IV. POLARIMETRY THEORETICAL ANALYSIS

The approach of this analysis is to use numerical examples to verify the TD theorems put forth by current researchers. The objective is to illustrate that full polarimetric data set does enhance target detection, simply by the fact that target information is lost in the target returns through the cross-pol channels that are not collected. Depending on the target geometry and orientation, the recovery of such information may be pivotal to the detection of the target.

The second aspect of the analysis is to create a Matlab model that can derive the optimal polarization states of the incident electric field for any target scattering matrix. There currently exist many analytical techniques to obtain the optimal polarization states and our implementation in Matlab provides a fast and easy numerical instantiation of the derived solutions.

The source codes for the two models are included in the appendices.

A.   USING TD THEOREMS FOR TARGET DETECTION

1.   Scattering Matrices and Vectors

Before we use the TD theorems in Chapter III, some verification was conducted to ensure commutability between the scattering matrix and scattering vector through known matrices of canonical targets, also introduced in Chapter 3.

Expressing equation (3.52) in terms of the elements of the scattering matrix yields

$$\begin{pmatrix} A_{HH} \\ A_{VV} \\ A_{HV} \end{pmatrix} = \frac{1}{2} \begin{pmatrix} \cos\alpha + \sin\alpha\cos\beta \\ \cos\alpha - \sin\alpha\cos\beta \\ \sin\alpha\sin\beta \end{pmatrix} \tag{4.1}$$

Starting with the sphere or the flat plate, the angle α is selected as 0^0 for an isotropic odd bounce surface while β can adopt any angle due to the symmetry of the sphere. Substituting this into the equation (4.1) we obtain

$$\begin{pmatrix} A_{HH} \\ A_{VV} \\ A_{HV} \end{pmatrix} = \frac{1}{2} \begin{pmatrix} \cos 0 + \sin 0 \cos \theta \\ \cos 0 - \sin 0 \cos \theta \\ \sin 0 \sin \theta \end{pmatrix} = \frac{1}{2} \begin{pmatrix} 1 \\ 1 \\ 0 \end{pmatrix} \tag{4.2}$$

or, in the more common scattering (normalized) form,

$$A_{sphere} = \begin{bmatrix} 1 & 0 \\ 0 & 1 \end{bmatrix} \tag{4.3}$$

This is in agreement with Table III-3 of scattering matrices of canonical targets.

Similarly for a dihedral orientated at an angle θ, the α angle is selected as a 90^0 for an isotropic even bounce surface, the scattering matrix elements are,

$$\begin{pmatrix} A_{HH} \\ A_{VV} \\ A_{HV} \end{pmatrix} = \frac{1}{2} \begin{pmatrix} \cos 90 + \sin 90 \cos 2\theta \\ \cos 90 - \sin 90 \cos 2\theta \\ \sin 90 \sin 2\theta \end{pmatrix} = \frac{1}{2} \begin{pmatrix} \cos 2\theta \\ -\cos 2\theta \\ \sin 2\theta \end{pmatrix} \tag{4.4}$$

$$A_{dihedral} = \begin{bmatrix} \cos 2\theta & \sin 2\theta \\ \sin 2\theta & -\cos 2\theta \end{bmatrix} \tag{4.5}$$

The above examples illustrates that the target scattering vector does connect the scattering matrix to the target geometry and scattering mechanism by appropriate selection of the α and β angles.

2. Construction of Foliage

Foliage commonly constitutes radar volume clutter and hides legitimate targets. It is an important aspect of radar detection to study and model this target/clutter interaction. The foliage is expected to bring about some degree of depolarization of the electric waves but this effect is not significant in any one single direction due to the random distribution and orientation of the leaves.

We use the same basic equation derived from TD analysis and, as before, model the foliage as a two-dimensional layer of leaves. The model is implemented in MatLab. Each leaf resides in a single cell in a grid of user-defined

dimensions (We use a 50 by 50 grid in this simulation). Each cell is then represented by a scattering vector or matrix. This concept is shown in Figure IV-1

$$L_{ij} = \begin{pmatrix} \cos \alpha_{ij} \\ \sin \alpha_{ij} \cos \beta_{ij} \\ \sin \alpha_{ij} \sin \beta_{ij} \end{pmatrix}$$
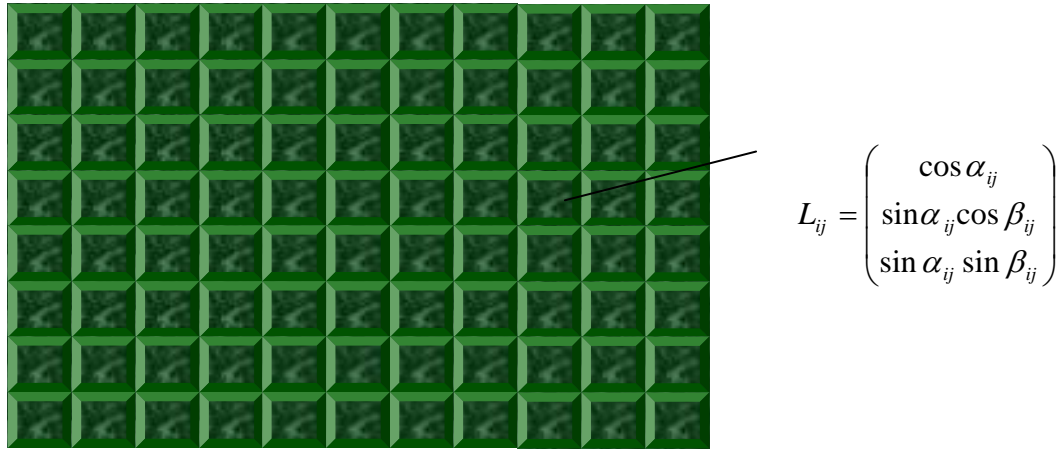
Figure IV-1 Foliage Modeling

The angle α is selected as 45^0 to simulate the leaves as a cloud of small anisotropic dielectric dipoles. The β angle is taken to be uniformly distributed from 0 to π to simulate the random orientation of the leaves. From the scattering vectors, we derive the scattering behavior and populate each cell with an appropriate scattering matrix.

Now, we introduce a propagating electric-field to interact with the foliage and then study the backscattered polarization states. Jones vectors are used to represent horizontally, vertically and circularly polarized E-fields.

Table IV-1 Jones Vectors of Incident E-fields

Horizontal Linear Polarization	$E_0 = \begin{bmatrix} 1 \\ 0 \end{bmatrix}$
Linearly Polarized at 45^0	$E_0 = \begin{bmatrix} \dfrac{1}{\sqrt{2}} \\ \dfrac{1}{\sqrt{2}} \end{bmatrix}$
Left Circular Polarization	$E_0 = \dfrac{1}{\sqrt{2}} \begin{bmatrix} 1 \\ j \end{bmatrix}$

The Jones vector will interact with each of the cells according to the following equation:

$$\begin{bmatrix} E_x^r \\ E_y^r \end{bmatrix} = \begin{bmatrix} A_{xx} & A_{xy} \\ A_{xy} & A_{yy} \end{bmatrix} \begin{bmatrix} E_x^i \\ E_y^i \end{bmatrix}$$

(4.6)

The output of our model is a graphical display of the horizontal and the vertical components of the backscattered E-field.

a)   *Horizontal Incident E-Field*

The plot shown below is the backscattered E-field due to a horizontally polarized incident E-field, $E^i = \begin{bmatrix} 1 & 0 \end{bmatrix}^T$.
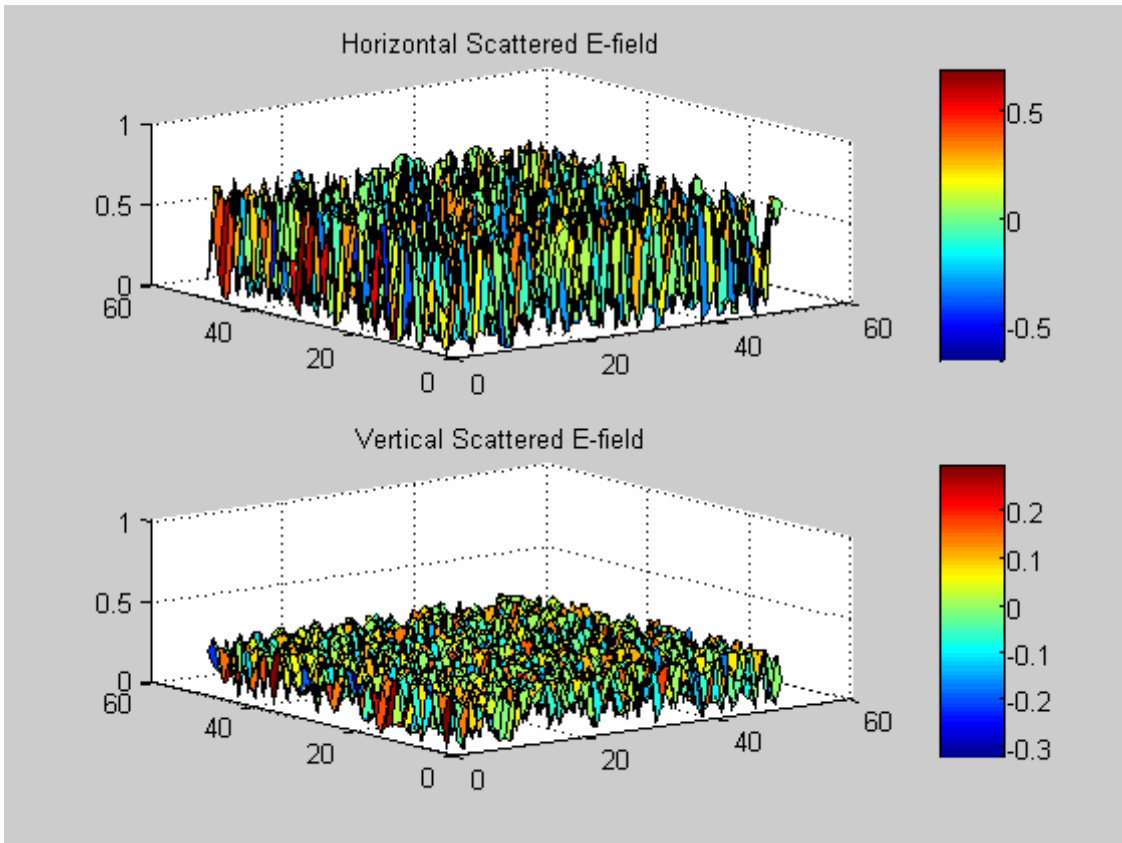
Figure IV-2 Backscattered E-field due to a Horizontally Polarized Incident E-field

The mean scattering matrix of the foliage from this simulation run is:

$$\bar{A}_{foliage} = \begin{bmatrix} 0.3514 & 0.2274 \\ 0.2274 & 0.3558 \end{bmatrix}$$

50

and the mean return of the electric-field is

$$\bar{E}^r = \begin{bmatrix} 0.3514 \\ 0.2274 \end{bmatrix}$$

These results show that some degree of depolarization has occurred as the completely horizontally polarized incident e-field is now depolarized by the foliage with backscattered E-field components in both vertical and horizontal polarized states.

b) Linearly Polarized at 45^0 Incident E-field

The simulation run was repeated with linearly polarized at 45^0 E-field with components of equal magnitude in both horizontal and vertical polarization state.
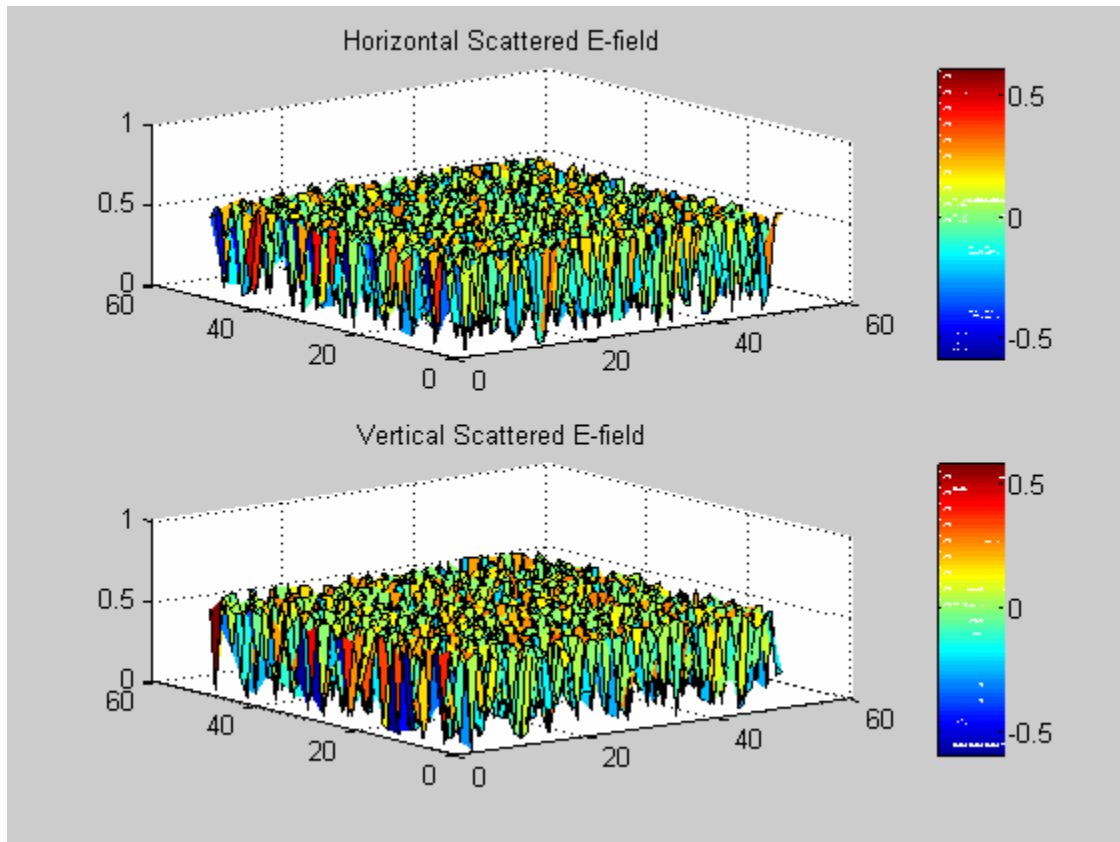
Figure IV-3 The Backscattered E-field from a Linearly Polarized at 45^0 E-field

The mean scattering matrix is identical to the last simulation and the mean backscattered E-field is now:

$$\bar{E}^r = \begin{bmatrix} 0.41 \\ 0.40 \end{bmatrix}$$

This result is to be expected since the incident E-field is equally polarized in the vertical and horizontal directions – the foliage being a random depolarizer, it should not have significant effect on the E-field polarization over sufficiently large sample.

c) Circularly-Polarized Incident E-field

Another interesting scenario that was examined used a circularly polarized incident electric field with the Jones vector, $E^i = \begin{bmatrix} \dfrac{1}{\sqrt{2}}, j\dfrac{1}{\sqrt{2}} \end{bmatrix}^T$ for a left circularly polarized incident field. The results for this case are presented in Figure (V-4) (both the real and imaginary parts of the echo field).

Figure IV-4 Backscattered E-field from a Left Circularly Polarized Incident E-field

The mean of the backscattered E-field is then

$$\bar{E}^r = \begin{bmatrix} 0.25 + j0.16 \\ 0.16 + j0.25 \end{bmatrix} \tag{4.7}$$

3. Modeling Target and Foliage

The idea now is to locate a target within the foliage and observe the overall scattering behavior. A number of canonical targets may be used: e.g. flat plates, dihedrals oriented at different angles or metallic helixes. The scattering vectors of the targets are l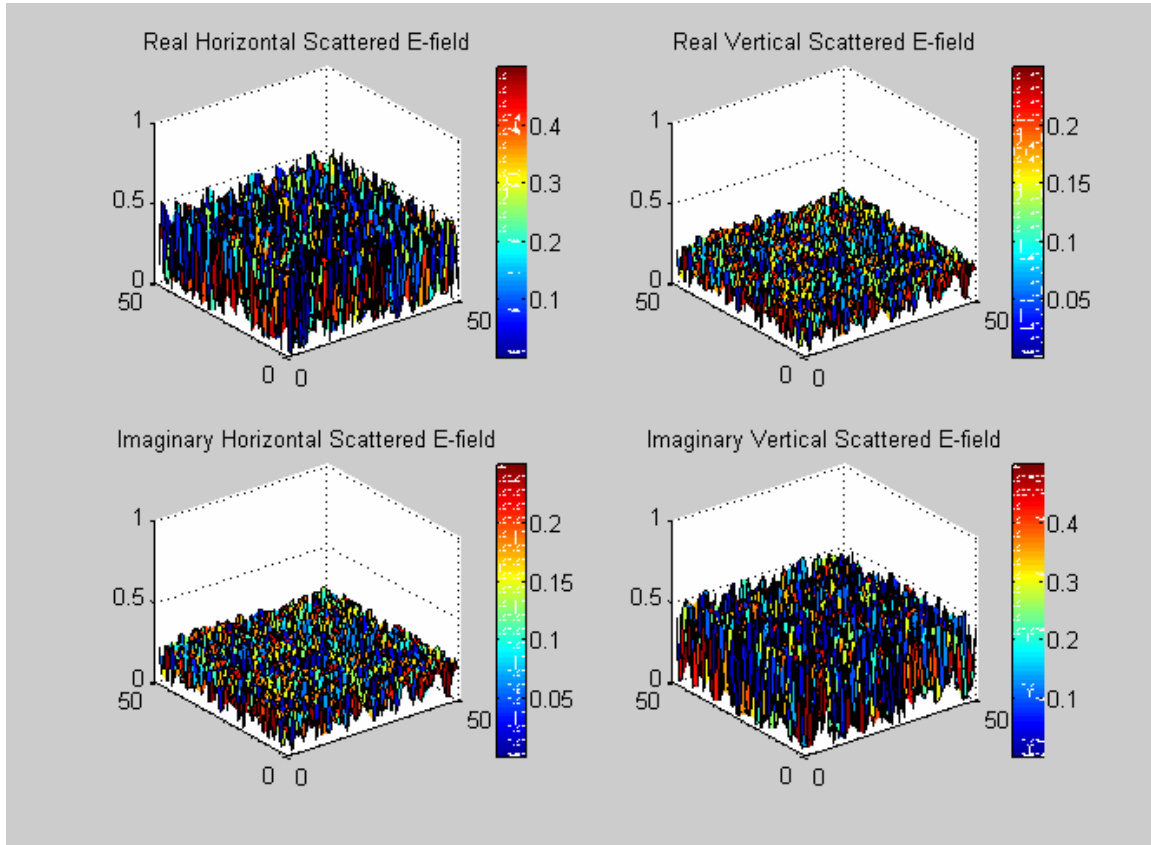isted in Table III-3. The location of the target is randomized in the 50 by 50 grid so that each simulation run is associated with a different target location. Figure IV-5 gives an illustration of the model.

Dihedral oriented at an angle located at a random location
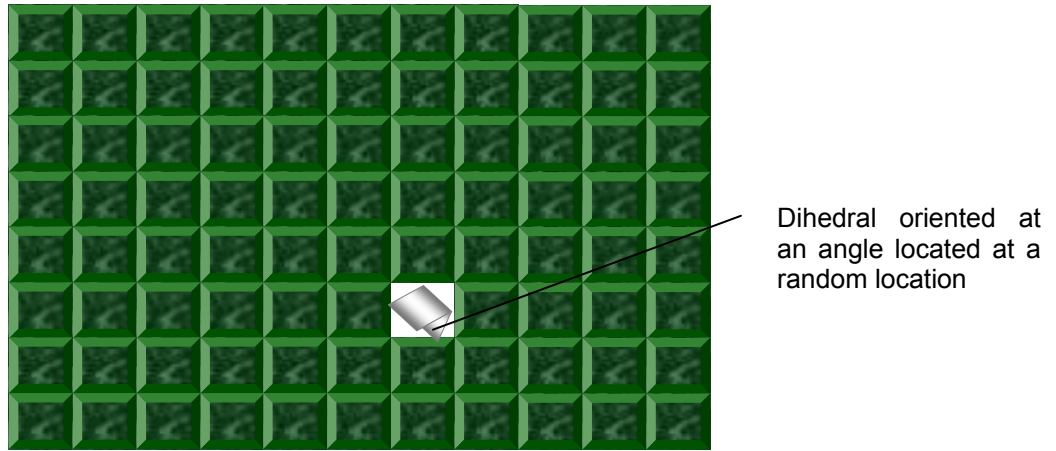
Figure IV-5 Modeling the Target and the Foliage Together

The model currently holds scattering matrices of most known canonical targets (including linear polarization at various orientations, dihedrals at various orientations, flat plates/ spheres and helixes) and Jones vectors of various polarizations of the incident E-fields.

The backscattered returns will now be due to both the foliage clutter and the target based on the following relationship

$$E^r = A_{target} E^i + A_{clutter} E^i \tag{4.8}$$

a)   *Horizontally Polarized Incident E-field on Flat Plate*

A relatively straight forward simulation run was conducted first based on the scenario of a horizontally polarized electric field impinging onto a flat plate target. The flat plate does not depolarized the incident electric field and

53

the reflected electric-field from the target alone is therefore still expected to be located in the horizontal component. The result of this simulation run is given in Figure IV-6.
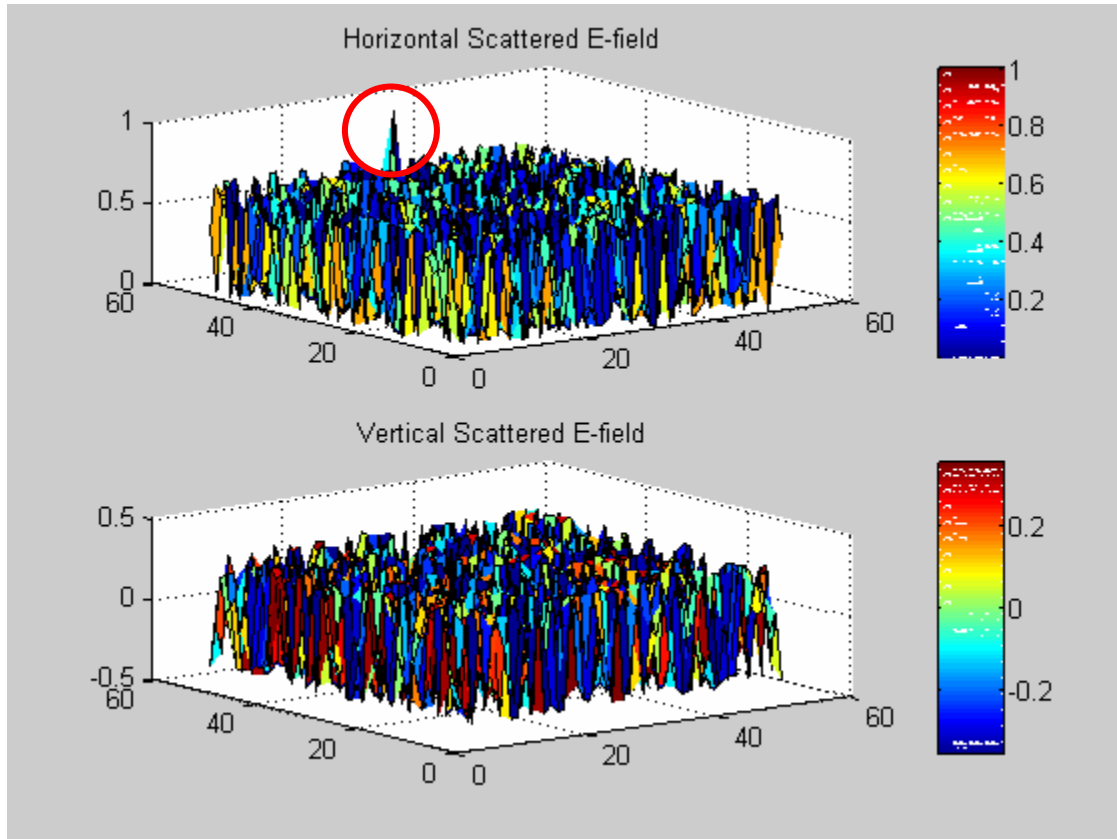
Figure IV-6 Backscattered E-field from a Horizontally Polarized Incident E-field reflected from a Flat Plate

As discussed, for this case the bright target return is not depolarized and is located within the horizontal components of the backscattered E-field, which is the same polarization of the transmitting antenna that produced the horizontally polarized incident field. The foliage behaves by altering the horizontal incident E-field so that the backscattered E-field has a vertical component. However, this behavior would be different if a depolarizing target is used.

b) *Horizontally Polarized E-field on 45⁰ Dihedral Target*

For the next simulation run a 45^0 oriented dihedral, known to completely depolarize the incident field, is examined. We continue to use a horizontally polarized incident field. The result obtained is shown in Figure IV-7
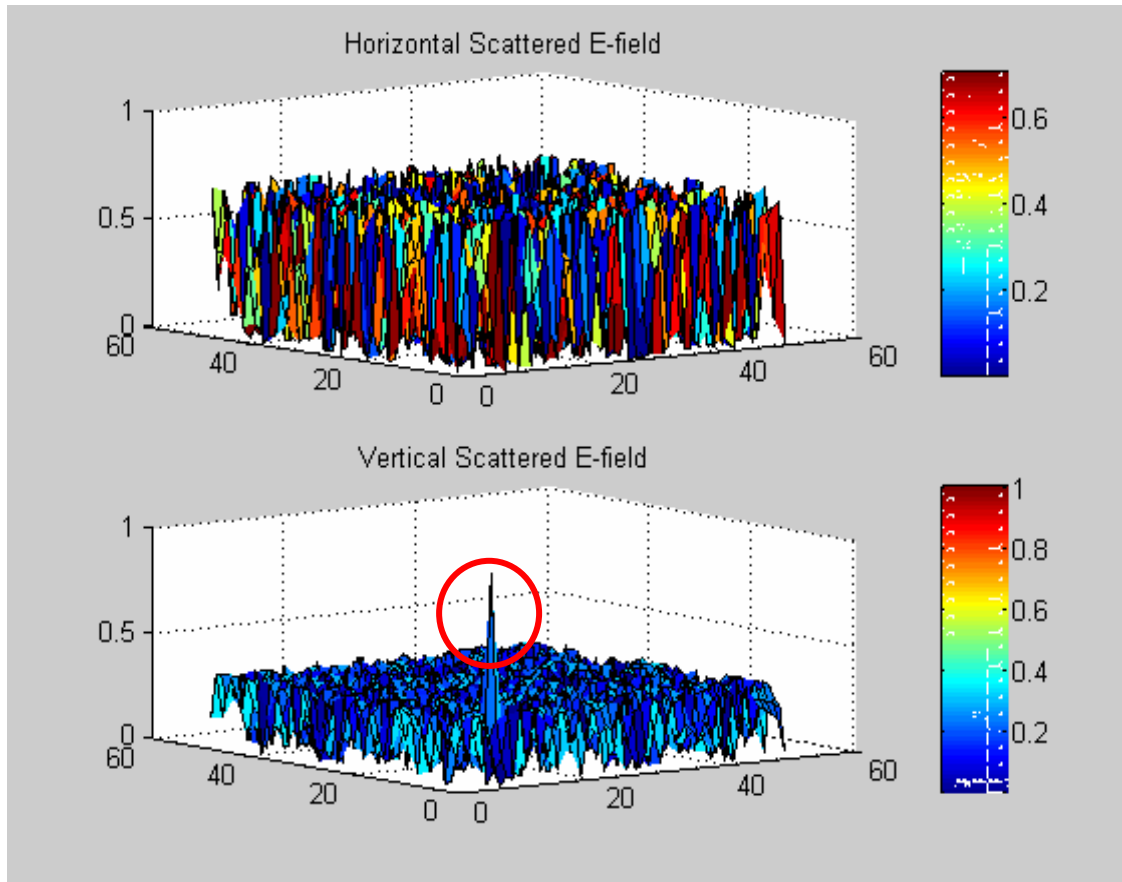
Figure IV-7 Backscattered E-field from a Horizontally Polarized Incident E-field reflected from a 45^0 Oriented Dihedral

Now the target return is completely located in the vertical component of the backscattered electric field. Hence without a full polarimetric data set, this target will not be detected despite producing such a bright (clutter-free) return.

c) *Left-Circularly Polarized E-field on Flat Plate Target*

The effect of circularly polarized incident E-field on various targets was also investigated using the model. The Jones vector of the incident E-field is now

$$E^i = \begin{bmatrix} \dfrac{1}{\sqrt{2}} \\ j\dfrac{1}{\sqrt{2}} \end{bmatrix}$$ (4.9)

and it represents a left-circularly polarized wave. The imaginary vertical component means that the two orthogonal components are 90^0 out of phase. The first scenario once again involves a flat plate target and the result of the simulation is shown in Figure IV-8 (including both the real and the imaginary components). The result essentially shows that the backscattered wave is not depolarized, and continues to be a circularly polarized wave (with real component in the horizontal and imaginary component in the vertical).
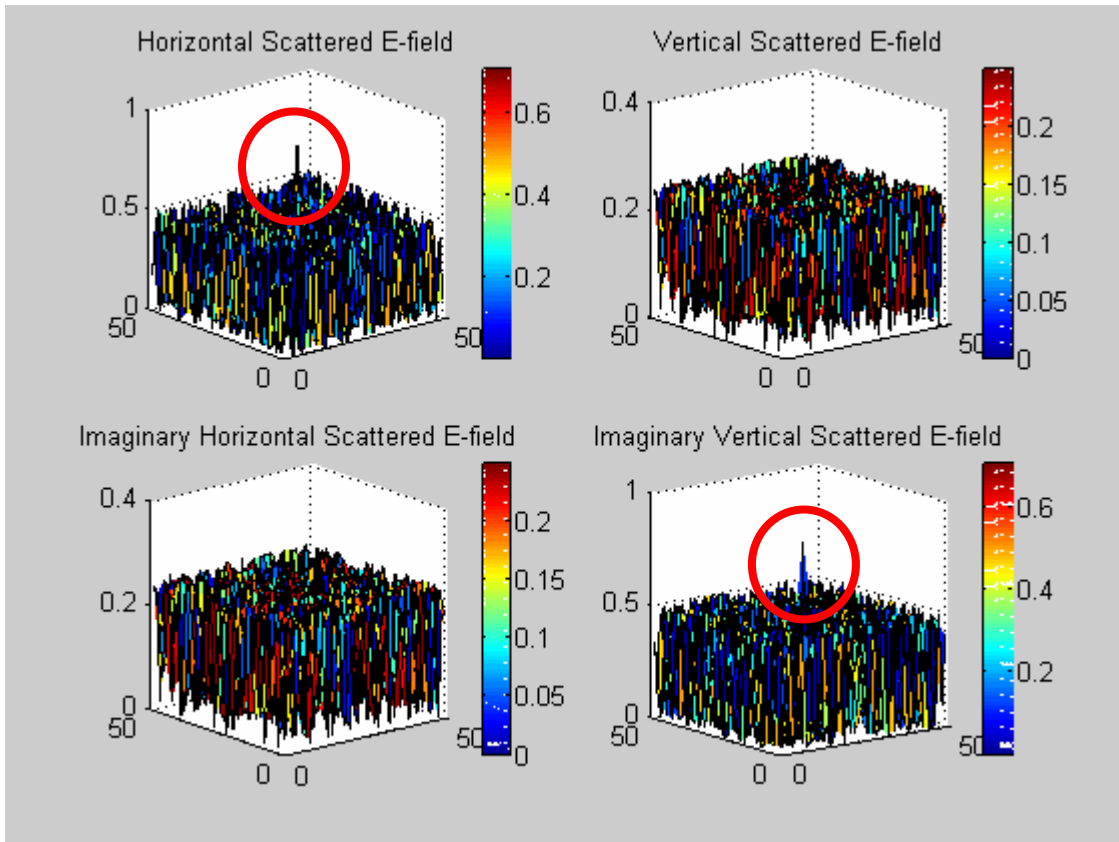
Figure IV-8 Backscattered E-field from a Left-Circularly Polarized Incident E-field reflected from a Flat Plate

d) *Left-Circularly Polarized E-field on Helix Target*

The last scenario included here is that of a circularly polarized E-field impinging on a helical target. The helical target acts as a polarizer that brings about a phase difference of 90^0 to the vertical and horizontal components of the incident E-field. Because the incident E-field components are already out of phase by 90^0, the helix target actually removes the phase difference resulting in a linearly polarized backscattered signal. This effect is shown in Figure IV-9. The backscattered signal is now a horizontally polarized wave.
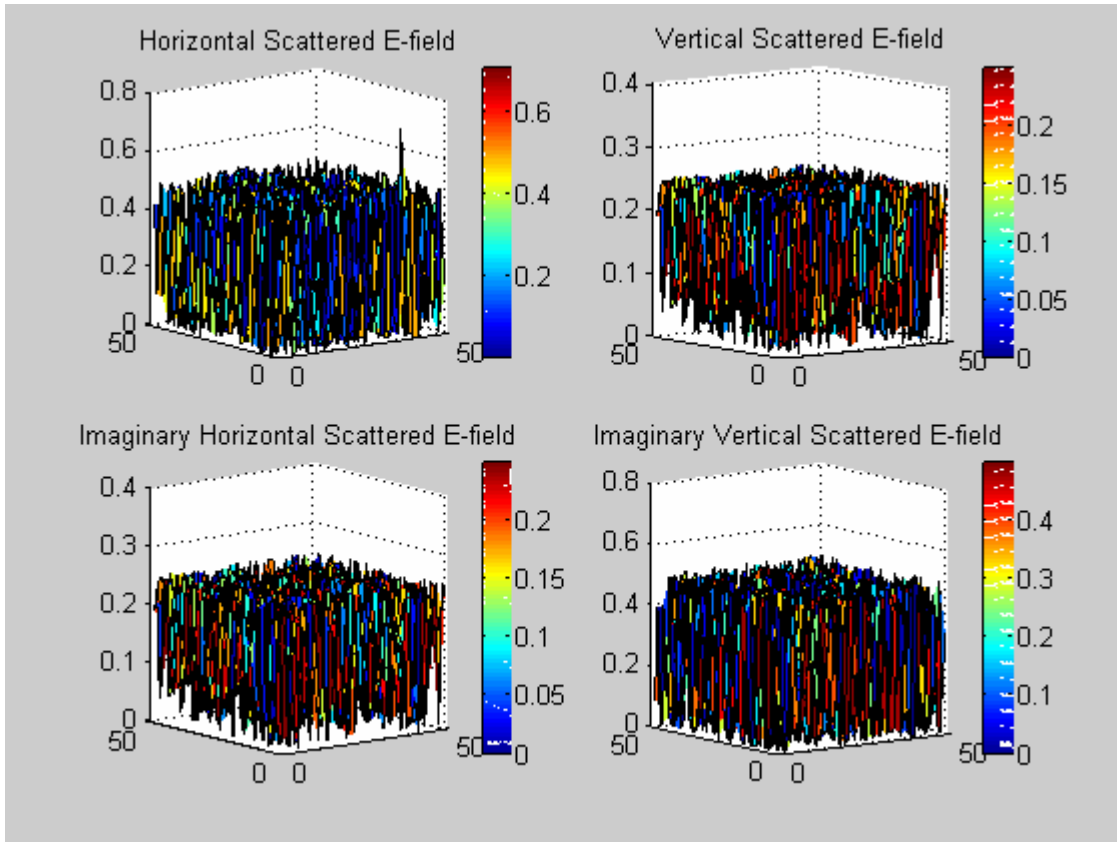
Figure IV-9 Backscattered E-field from a Left-Circularly Polarized Incident E-field reflected from a Helix

This portion of the analysis shows the possibility of using TD theorems to extract physical properties of targets from their scattering matrices and these physical attributes can be used in modeling – in this particular case, for simulation of foliage. The latter example of a man-made target buried in foliage clutter demonstrates the importance of obtaining full polarimetric data set

for target detection. We chose a particularly bright target and showed that, due to depolarization, the return signal can be completely lost. It should also be noted that for the dihedral, the characteristic to depolarize also depends on its geometry, i.e., its orientation angle of 45^0.

B.   POLARIZATION OPTIMIZATION

The theory for optimization of polarization state is detailed in [1] and a number of techniques are discussed there. For simulation in Matlab, we select an optimization technique that uses the Stokes vectors and the Mueller (power) matrix. This technique has the particular advantage that the input arguments are in the power or intensity units, so that the output, which is also in terms of power units, can be directly obtained by selecting the appropriate elements of the Mueller matrix. Since the program will essentially vary the input parameters until the peak power return is obtained, the intermediate mathematical techniques covered in [1] can be avoided entirely.

1.   Modeling the Varying Incident Electric Field and Stokes Vectors

The polarization states of the incident electric field can be described complete by its tilt and ellipticity angles (refer to Chapter 2 Section B). Equation (3.6) shows the relationship as [8]

$$E_{(x,y)} = Ae^{-j\delta}\begin{bmatrix} \cos\varphi & -\sin\varphi \\ \sin\varphi & \cos\varphi \end{bmatrix}\begin{bmatrix} \cos\tau \\ j\sin\tau \end{bmatrix} \tag{4.10}$$

Hence, any Jones vector of the electric field may be described by varying the tilt and the ellipticity. However, as defined by the polarization ellipse, the ellipticity has a range of -45^0 to 45^0 while the tile of the ellipse has a range of 0^0 to 180^0 – and these will be the ranges of our model parameters.

The electric field is used to generate the Stokes vectors using the following equation [11]

58

$$\begin{bmatrix} S_0 \\ S_1 \\ S_2 \\ S_3 \end{bmatrix} = \begin{bmatrix} |E_x|^2 + |E_y|^2 \\ |E_x|^2 - |E_y|^2 \\ 2|E_x||E_y|\cos\delta \\ 2|E_x||E_y|\sin\delta \end{bmatrix} \tag{4.11}$$

where δ is the phase difference between the x (horizontal) and y (vertical) components of the electric field and can be derived from the tilt and/or ellipticity angles [12]

$$\cos\delta = \tan 2\varphi \frac{|E_x|^2 - |E_y|^2}{2|E_x|} \tag{4.12}$$

2. Application of the Mueller (Power) Matrix

In Chapter III we explained how the Mueller matrix transforms the incident Stokes vectors to the backscattered Stokes vectors, analogously to the operation of scattering matrix and Jones vectors. However, we need to separate the backscattered field into the co-polarized and the cross-polarized channels to explore the effects of polarization, i.e., we need to determine how much of the incident power is depolarized and returns in the orthogonal component (which is collected only a full polarimetric data set).

This is done by generating two Mueller matrices, one each for the co-pol and the cross-pol channel, in a manner based on developments by Boerner [1],

$$M_c = \begin{bmatrix} 1 & 0 & 0 & 0 \\ 0 & 1 & 0 & 0 \\ 0 & 0 & 1 & 0 \\ 0 & 0 & 0 & -1 \end{bmatrix} M \tag{4.13}$$

$$M_x = \begin{bmatrix} 1 & 0 & 0 & 0 \\ 0 & -1 & 0 & 0 \\ 0 & 0 & -1 & 0 \\ 0 & 0 & 0 & 1 \end{bmatrix} M \tag{4.14}$$

Then, the co-pol and cross-pol power can be obtained from the following equations [1]

$$P_c = \frac{\left[S^i \right]^T \left[M_c \right] \left[S^i \right]}{\left\| S \right\|}$$ (4.15)

$$P_x = \frac{\left[S^i \right]^T \left[M_x \right] \left[S^i \right]}{\left\| S \right\|}$$ (4.16)

3.   Results and Analysis

The model can now be used to determine the polarization state for maximum power return for any target scattering matrix. The choice of polarization state of the incident electric field ensures a maximum return in either the co-polarized or the cross-polarized channel. In this sense, if the target characteristics can be determined, and a full polarimetric data set is available, the transmitted electric field can be selected to optimize the power return.

The first scattering matrix used for simulation was that of a flat plate (or a sphere) that does not depolarize the incident wave field. The result of the simulation is presented in Figure IV-10.
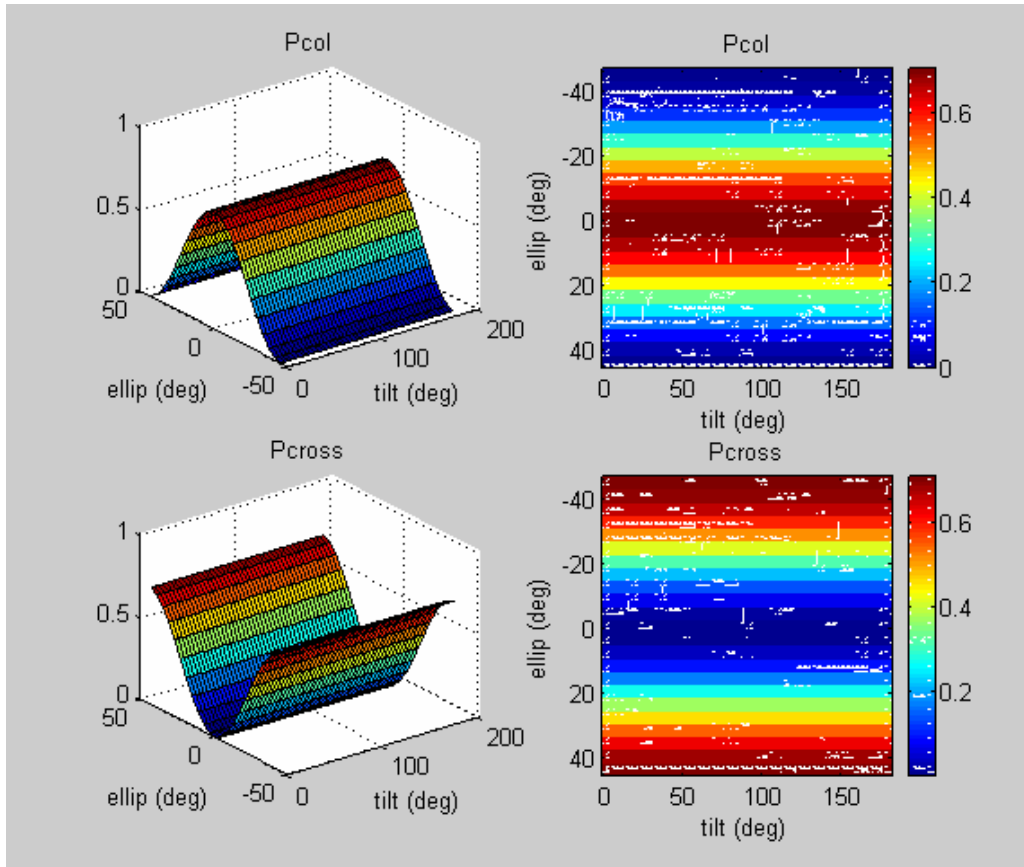
Figure IV-10 Backscattered Power for a Flat Plate

The figures in the first row show the power return in the co-polarized channel that has the same polarization state as the antenna transmitting and receiving the signal (for the mono-static case). The power is plotted as a function of the tilt and ellipticity angles. The figure on the left gives a three-dimensional presentation while the right figure gives a two-dimensional projection in which the gradient of the color gives the power return. The figures in the second row give the results for the cross-polarized channel.

The results show that the return power depends only on the ellipticity angle and not the tilt angle. For a 0^0 ellipticity angle, the electric field is linearly polarized and the maxima occurs in the co-polarized channel showing maximum power is backscattered with the same polarization as the transmitting antenna. As the ellipticity increases to, say 10^0, the co-pol power begins to drop, similar to

the co-pol power of the incident E-field. When the ellipticity is increased to its maximum of 45^0, the cross-pol power attains its maximum value.
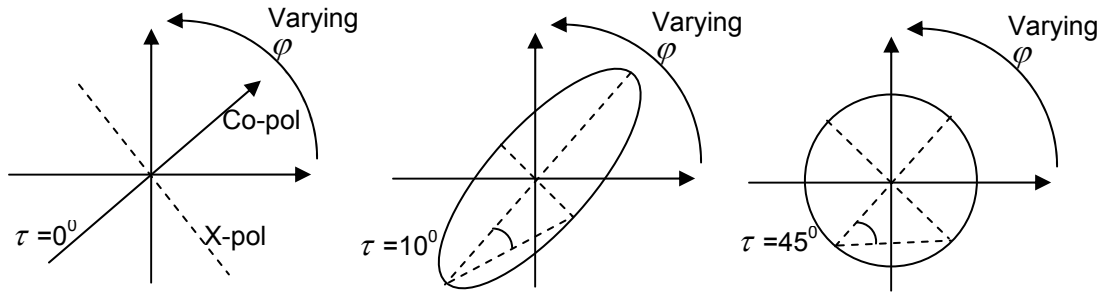
Figure IV-11 Variation of Co-pol and Cross-pol Powers with Ellipticity

This behavior shows that the target does not depolarize the incident field at all. This result is expected for a flat plate target and hence, the model has accurately simulated this behavior.

The next scattering matrix used for simulation was that of the 45^0 oriented dihedral that completely depolarizes the incoming electric field. The appropriate scattering matrix is

$$A_{45^0\,dihedral} = \begin{bmatrix} 0 & 1 \\ 1 & 0 \end{bmatrix} \qquad (4.17)$$

The results of the simulation is presented in Figure IV-12 below.
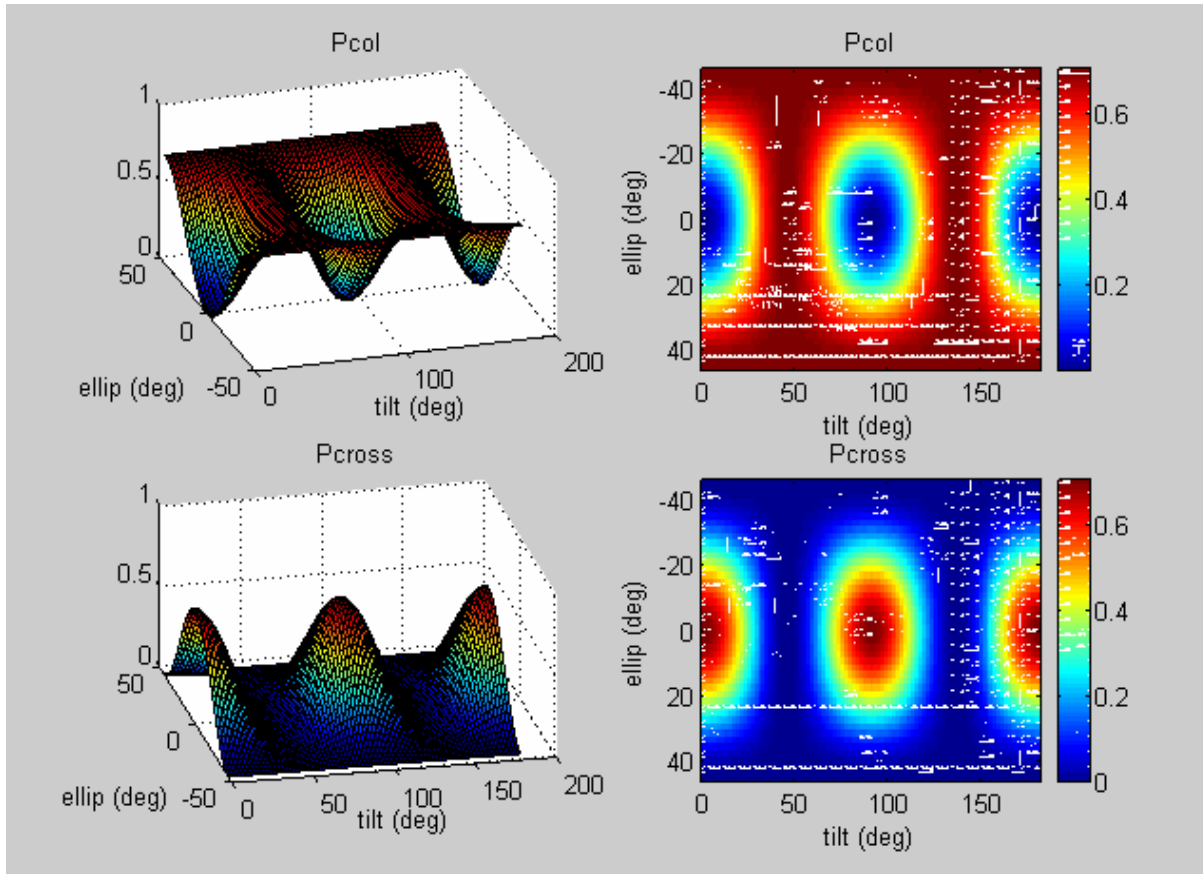
Figure IV-12 Backscattered Power for Dihedral Oriented at 45^0

The results given in Figure IV-12 show that the co-pol nulls are the cross-pol peaks. We identify the tilts and ellipticity whereby the cross pol peaks occur.

Table IV-2 Incident Electric Fields for Cross-Pol Peaks

Tilt, φ	Ellipticity, τ	Equivalent Jones
0^0	0^0	$\begin{bmatrix} 0 \\ 1 \end{bmatrix}$
90^0	0^0	$\begin{bmatrix} 1 \\ 0 \end{bmatrix}$

We can conclude from the simulation results that horizontally and vertically polarized electric fields are completely depolarized by a 45^0 oriented dihedral.

The last scattering matrix that we present here is

$$A = \begin{bmatrix} 2j & 0.5 \\ 0.5 & -j \end{bmatrix}$$

(4.18)

This is an arbitrary target obtained from [1] that is used to ensure the model is accurate and the results are in agreement with the reference. This case is included here because it represents a complex target and gives rise to a more complicated returned power signal, illustrated in the figure below.

Figure IV-13 Backscattered Power for an Arbitrary Target

C. FURTHER WORK

Even though most existing tactical radar systems are not polarimetric, future tactical radars are expected to exploit polarization information. The current thesis serves as a review of polarimetric investigations as it provides a comprehensive summary of the current efforts and development in polarimetry

theories. In particular, two of the more useful and interesting theories on TD theorems and optimization have been examined at a level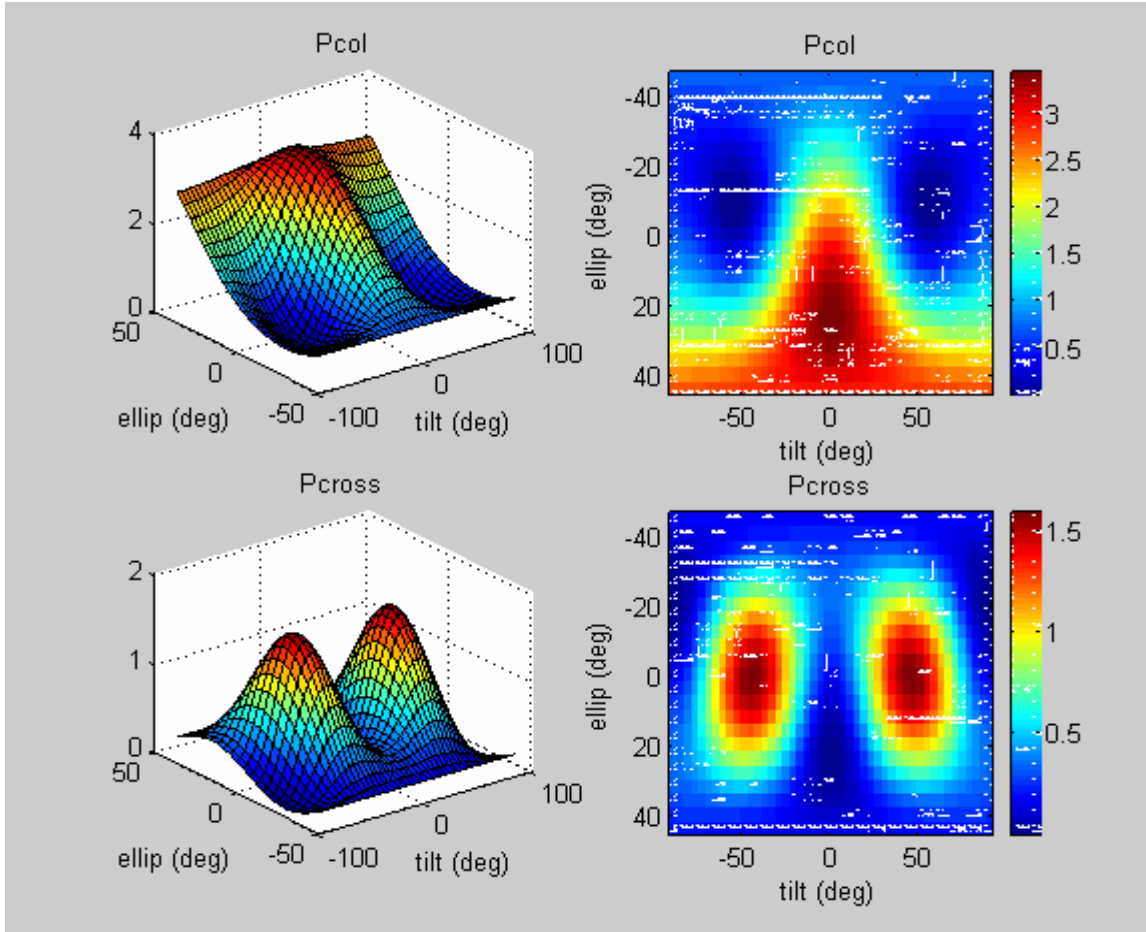 sufficient to verify them. Given the fact that most of these polarimetry theories are recent developments (dating back, in some cases, to research programs begun in the late 70s), many aspects of the proposed theories can be further investigated, developed or verified.

For the current investigation, a more complex foliage clutter model can be introduced. For cultured vegetation, there exists some degree of correlation such that the scattering mechanism and the orientation of the leaves may not be completely random. The correlation may be introduced in the α angle of the TD theorems from the 'P' intensities in the entropy. A more realistic model can also be achieved if it is extended to the third dimension by introducing tree trunks beneath the foliage. The trunks are expected to have a single or a slightly varying orientation. Finally, since the current model is based on theoretical analysis, some realism can be injected if it can be compared to real or existing data.

If existing full polarimetric data sets can be obtained, an interesting problem would be to analyze the returns, decompose the scattering mechanisms and create a color plot based on different scattering mechanisms. An example would be the Pauli decomposition plot given in Figure III-6.

Another particularly useful implementation of radar polarimetry is in the interferometry of Synthetic Aperture Radar (POLINSAR). This is an ongoing research topic by current researchers such as Cloude and Boerner. The idea is that the coherency of interferometry data sets from multipass SAR (both temporal and spatial decorrelation) depends strongly on the polarization states. Cloude developed a methodology whereby polarimetric transformation bases can be used to analyze SAR interferograms so that the coherency can be optimized.

THIS PAGE INTENTIONALLY LEFT BLANK

APPENDIX   MATLAB SOURCE CODES

A.   SOURCE CODE FOR TD THEOREMS

```
clear all
%Suite of EM-waves (From Ref [12])
%E=[1/sqrt(2);1/sqrt(2)];                    %linearly polarized at 45degree
E=[1;0];                                     %horizontally polarized
%E=[0;1];                                    %verticallly polarized
%E=[1/sqrt(2);(1/sqrt(2))*j]                 %Left circular polarized
%E=[1/sqrt(2);-(j*1/sqrt(2))]                %Right circular polarized

% Defined alpha angle: scattering mechanism
alpha_l = 45;                                %45 degrees for dipole
alpha_l_rad = alpha_l/180*pi;                %convert to radians

%Assign random target location
target_x =round(rand*50);
target_y =round(rand*50);

%Create scene
for x_space=1:50;
for y_space=1:50;

%Create clutter model for each locations
beta_l_rad = rand*pi;
%Assign leaves orientation (From Ref [4])
k_l=[cos(alpha_l_rad);sin(alpha_l_rad)*cos(beta_l_rad);sin(alpha_l_rad)*sin(beta
_l_rad)]; % leaves model
s_hh=(k_l(1,1)+ k_l(2,1))/2;                 %clutter scattering matrix
s_vv=(k_l(1,1)- k_l(2,1))/2;                 %clutter scattering matrix
s_x=k_l(3,1)/2;                              %clutter scattering matrix
S(x_space,y_space,1)=[s_hh];                 %clutter scattering matrix
S(x_space,y_space,2)=[s_x];                  %clutter scattering matrix
S(x_space,y_space,3)=[s_x];                  %clutter scattering matrix
S(x_space,y_space,4)=[s_vv];                 %clutter scattering matrix

%EM wave depolarized by Clutter
s_c =[s_hh,s_x;s_x,s_vv];
e_clutter = s_c*E;

%Add effect of dihedral/helix/flat plate at predetermined location
if (x_space==target_x) & (y_space==target_y)
   %s_t =[sqrt(2)/2,sqrt(2)/2;sqrt(2)/2,-sqrt(2)/2];    %dihedral at 22.5 deg
   s_t = [0,1;1,0];                                     %dihedral at 45 deg
   %s_t = [0.5,-j*0.5;-0.5,-j*0.5];                     %metallic helix
```

```matlab
    %s_t= [1,0;0,1];                                          %flat plate
    %s_t= [1,0;0,-1];                                         %dihedral at 0 degree
   E_t =s_t*E;

%Sum clutter and dihedral at where the target is located
   E_clutter(x_space,y_space,1)= E_t(1,1); %+ e_clutter(1,1);
   E_clutter(x_space,y_space,2)= E_t(2,1); %+ e_clutter(2,1);

else
   E_clutter(x_space,y_space,1)=e_clutter(1,1);
   E_clutter(x_space,y_space,2)=e_clutter(2,1);
end

end
end

%Read out of results
mean(mean(S(:,:,1)))           %scattering matrix
mean(mean(S(:,:,2)))           %scattering matrix
mean(mean(S(:,:,3)))           %scattering matrix
mean(mean(S(:,:,4)))           %scattering matrix
mean(mean(E_clutter(:,:,1)))   %Back scattered E-field
mean(mean(E_clutter(:,:,2)))   %Back scattered E-field

%plots for real values
[x,y] = meshgrid([1:50]);
Z_h = E_clutter(:,:,1);
subplot(2,2,1), surf(x,y,real(Z_h)), title('Horizontal Scattered E-field')
colorbar

Z_v = E_clutter(:,:,2);
subplot(2,2,2), surf(x,y,real(Z_v)), title('Vertical Scattered E-field')
colorbar

%imaginary plots
[x,y] = meshgrid([1:50]);
Z_h = E_clutter(:,:,1);
subplot(2,2,3), surf(x,y,imag(Z_h)), title('Imaginary Horizontal Scattered E-field')
colorbar

Z_v = E_clutter(:,:,2);
subplot(2,2,4), surf(x,y,imag(Z_v)), title('Imaginary Vertical Scattered E-field')
colorbar
```

B. SOURCE CODE FOR POLARIZATION OPTIMIZATION

```
clear all
t=1;                                        %counter

%Target Scattering Matrices
S=[2j,0.5;0.5,-j];                          % Arbitrary matrix from Ref [1]
%S=[1,0;0,1];                               %Sphere
%S=[1,0;0,-1];                              %Dihedral
%S = [0,1;1,0];                             %dihedral at 45 deg
 %S = [0.5,-j*0.5;-0.5,-j*0.5];             %metallic helix

%Transitional Matrices (From Ref [1])
C=0.5*[1,0,0,0;0,1,0,0;0,0,1,0;0,0,0,-1];   %Produces the Co-pol Mueller
X=0.5*[1,0,0,0;0,-1,0,0;0,0,-1,0;0,0,0,1];  %Produces the Crosspol Mueller
A=[1,0,0,1;1,0,0,-1;0,1,1,0;0,j,-j,0];      %Kronecker expansion matrix


for tilt=-0:2:180;                          %range of tilt angle
tilt_rad=(tilt/180)*pi;                     %convert tilt to radians
e=1;                                        %counter

for ellip=-45:2:45;                         %range of ellipticity angle
   ellip_rad=(ellip/180)*pi;                %convert to radian

%Contruct the incident E-field based on the current tilt and ellipticity (From Ref
[8])
 %To be used to generate the Stokes parameters
   E_i=[cos(tilt_rad)*cos(ellip_rad)-
sin(tilt_rad)*(j*sin(ellip_rad));sin(tilt_rad)*cos(ellip_rad)+cos(tilt_rad)*(j*sin(ellip_ra
d))];

   %Contruct Mueller matrices from the current scattering matrix
   %To be used for transforming incident Stokes parameters to backscattered
ones
   M =A*(kron(S,conj(S)))*inv(A);           %general Mueller
   Mc=C*M;                                  %Col-pol matrix
   Mx=X*M;                                  %Cross-pol matrix

   %Contruct the Stoke Parameters from the incident E-field (From Ref [11])
   g0=abs(E_i(1,:)^2)+ abs(E_i(2,:)^2);
   g1=abs(E_i(1,:)^2)- abs(E_i(2,:)^2);
   g2=(abs(E_i(1,:)^2)- abs(E_i(2,:)^2))*tan(2*tilt_rad);
   g3=(abs(E_i(1,:)^2)+ abs(E_i(2,:)^2))*sin(2*ellip_rad);
   gt=[g0;g1;g2;g3];

   %Derived the backscattered Stokes using the Mueller on the incident Stokes
```

```
    %Deriving the cross pol and copol powers
    power_col=transpose(gt)*Mc*gt/norm(gt,'fro');
    power_cross=transpose(gt)*Mx*gt/norm(gt,'fro');
    Pc(e,t)=power_col;                              %data stored as array
    Px(e,t)=power_cross;                            %data stored as array
    e=e+1;                                          %counter
end

t=t+1;                                             %counter
end

%Plots
a=-0:2:180;
b=-45:2:45;
[X,Y] = meshgrid([-0:2:180],[-45:2:45]);
subplot(2,2,1),surf(X,Y,Pc), title('Pcol'),xlabel('tilt (deg)'),ylabel('ellip (deg)')
subplot(2,2,2),imagesc(a,b,Pc), title('Pcol'),xlabel('tilt (deg)'),ylabel('ellip (deg)')
colorbar
subplot(2,2,3),surf(X,Y,Px), title('Pcross'),xlabel('tilt (deg)'),ylabel('ellip (deg)')
subplot(2,2,4),imagesc(a,b,Px), title('Pcross'),xlabel('tilt (deg)'),ylabel('ellip (deg)')
colorbar

% Readout of values
[A,B]=find(Px==(max(max(Px))))              %find  ellip  &  tilt  where
maxima occurs
```

LIST OF REFERENCES

[1]   Boerner W.-M., Yan W.-L., Xi A.-Q. and Yamaguchi Y., "On the Basic Principles of Radar Polarimetry: the Target Characteristic Polarization State theory of Kennaugh, Huynen's Polarization Fork Concept, and its Extension to the Partially Polarization Case"

[2]   Boerner W.-M., El-Arni M. B., Chan C.-Y. and Mastoris P. M., "Polarization Dependence in Electromagnetic Inverse Problems", IEEE Transactions on Antenna and Propagation, Vol. AP-29, Np. 2, March 1981

[3]   Cantrell D.C. "Partial Polarization", The University of Texas at Dallas, EE6334 Course Notes

[4]   Cloude S. R., Papathanassiou K. P., "Polarimetric SAR Interferometry", IEEE Transactions on Geoscience and Remote Sensing, Vol. 36, No. 5, September 1998

[5]   Cloude S. R., Pottier E., "A Review of Target Decomposition Theorems in Radar Polarimetry", IEEE Transactions on Geoscience and Remote Sensing, Vol. 34, No 2, March 1996

[6]   Cloude S. R., Pottier E., "An Entropy Based Classification Scheme for Land Applications of Polarimetric SAR", IEEE Transactions on Geoscience and Remote Sensing, Vol 35, No. 1 January 1997

[7]   Cloude S. R., Pottier E., "Concept of Polarization Entropy in Optical Scattering", Optical Engineering, Vol. 34, No. 6, June 1995

[8]   Germond A.-L., Pottier E. and Saillard J., "Bistatic Radar Polarimetry Theory"

[9]   Hellmann M. P. "SAR Polarimetry Tutorial (Beta version 0.1a)", http://epsilon.nought.de/, August 04

[10]   Mahafza B.R., "Radar Systems Analysis and Design Using Matlab", Chapman & Hall/ CRC, 2000

[11]   Mott H., "Polarization in Antennas and Radars", John Wiley & Sons, Inc., 1986

[12]   Pedrotti F. L. and Pedrotti L. S., "Introduction to Optics, 2nd Edition", Prentice Hall, 1993

[13]   Peebles P. Z., "Radar Principles", John Wiley & Sons, Inc., 1998

[14]   Ruck G. T., Barrick D. E., Stuart W. D., Krichbaum C. K., "Radar Cross Section Handbook, Volume 2", Plenum Press, 1970

[15]   Rudolf, H., "Increase of Information by Polarimetric Radar Systems", Institut für Höchstfrequenztechnik und Elektronik Universität Karlsruhe (TH), 2000

[16]   Sadiku, M. "Elements of Electromagnetism", Oxford University Press, Inc., 2001

[17]   Skolnik M. I., "Introduction to Radar Systems", McGraw-Hill Science/Engineering/Math, 2002

[18]   University of Zurich, Department of Geography, "Polarimetric SAR Interferometry (Pol-InSAR)", http://www.geo.unizh.ch/rsl/research/SARLab/SAR_PolInSAR/, October 04

[19]   Wikipedia Encyclopedia, http://en.wikipedia.org/, October 04

INITIAL DISTRIBUTION LIST

1. Defense Technical Information Center
    Ft. Belvoir, Virginia

2. Dudley Knox Library
    Naval Postgraduate School
    Monterey, California

3. Professor Brett Borden
    Physics Department
    Naval Postgraduate School
    Monterey, California

4. Professor Donald Walters
    Physics Department
    Naval Postgraduate School
    Monterey, California

5. Professor Yeo Tat Soon
    Temasek Defence Systems Institute
    Singapore

6. Ms Yong Siow Yin
    Defence Science and Technology Agency
    Singapore